Analyst

ROYAL SOCIETY OF CHEMISTRY

CRITICAL REVIEW

Nanozyme-based electrochemical biosensors for disease biomarker detection

Cite this: DOI: 10.1039/d0an00558d

Rabbee G. Mahmudunnabi, †[a] Fatema Zerin Farhana,†[b] Navid Kashaninejad,[c] Shakhawat H. Firoz, *[b] Yoon-Bo Shim*[d] and Muhammad J. A. Shiddiky *[c,e]

In recent years, a new group of nanomaterials named nanozymes that exhibit enzyme-mimicking catalytic activity has emerged as a promising alternative to natural enzymes. Nanozymes can address some of the intrinsic limitations of natural enzymes such as high cost, low stability, difficulty in storage, and specific working conditions (*i.e.*, narrow substrate, temperature and pH ranges). Thus, synthesis and applications of hybrid and stimuli-responsive advanced nanozymes could revolutionize the current practice in life sciences and biosensor applications. On the other hand, electrochemical biosensors have long been used as an efficient way for quantitative detection of analytes (biomarkers) of interest. As such, the use of nanozymes in electrochemical biosensors is particularly important to achieve low cost and stable biosensors for prognostics, diagnostics, and therapeutic monitoring of diseases. Herein, we summarize the recent advances in the synthesis and characterization of common nanozymes and their application in electrochemical biosensor development. After briefly overviewing the applications of nanozymes in non-electrochemical-based biomolecular sensing systems, we thoroughly discuss the state-of-the-art advances in nanozyme-based electrochemical biosensors, including genosensors, immunosensors, cytosensors and aptasensors. The applications of nanozymes in microfluidic-based assays are also discussed separately. We also highlight the challenges of nanozyme-based electrochemical biosensors and provide some possible strategies to address these limitations. Finally, future perspectives on the development of nanozyme-based electrochemical biosensors for disease biomarker detection are presented. We envisage that standardization of nanozymes and their fabrication process may bring a paradigm shift in biomolecular sensing by fabricating highly specific, multi-enzyme mimicking nanozymes for highly sensitive, selective, and low-biofouling electrochemical biosensors.

Received 19th March 2020,
Accepted 9th May 2020

DOI: 10.1039/d0an00558d

rsc.li/analyst

1. Introduction

The term "nanozymes" was first introduced by Pasquato and co-workers in 2004 to describe the ribonuclease-like activity of triazacyclononane functionalized gold nanoparticles (NPs) in the transphosphorylation reaction.[1] The definition of nanozymes has been solidified as enzyme-mimicking nanomaterials after the demonstration of the intrinsic peroxidase-like activities of magnetite (Fe_3O_4) NPs in 2007.[2,3] Since then, hundreds of nanomaterials have been reported with enzyme-mimicking properties along with diverse applications. Nanozymes have shown considerable advantages over natural enzymes due to their high and tunable catalytic activities, ease of modification, large surface area, low cost, and large-scale production. As such, nanozymes are widely regarded as direct alternatives to natural enzymes. Along with enzyme-mimicking activities, optical, electrical, and magnetic properties of certain nanozymes are ideal for most analytical applications. These characteristics greatly facilitate the integration and automation of multiple processes such as separation and detection procedures of molecular targets with immensely high speed, leading to a decrease in the preparatory steps and required time.[2,4,5] Fig. 1 summarizes the unique features of nanozymes and their applications in electrochemical sensors.

Tremendous advancements in nanotechnology have contributed significantly to the unprecedented growth and applications of nanozymes. These synergistic advances have led to the development of high-performance and ultra-sensitive platforms, including colorimetric, fluorometric, chemilumines-

[a]*Department of Molecular Science Technology, Pusan National University, Busan 46241, South Korea*
[b]*Department of Chemistry, Bangladesh University of Engineering and Technology, Dhaka, Bangladesh. E-mail: shfiroz@chem.buet.ac.bd*
[c]*Queensland Micro and nanotechnology Centre, Griffith University, Nathan Campus, QLD 4111, Australia. E-mail: m.shiddiky@griffith.edu.au*
[d]*Department of Chemistry & Institute of BioPhysio-Sensor Technology, Pusan National University, Busan 46241, South Korea. E-mail: ybshim@pusan.ac.kr*
[e]*School of Environment and Science, Griffith University, Nathan Campus, QLD 4111, Australia*
† Equal contributor and first-named authors.

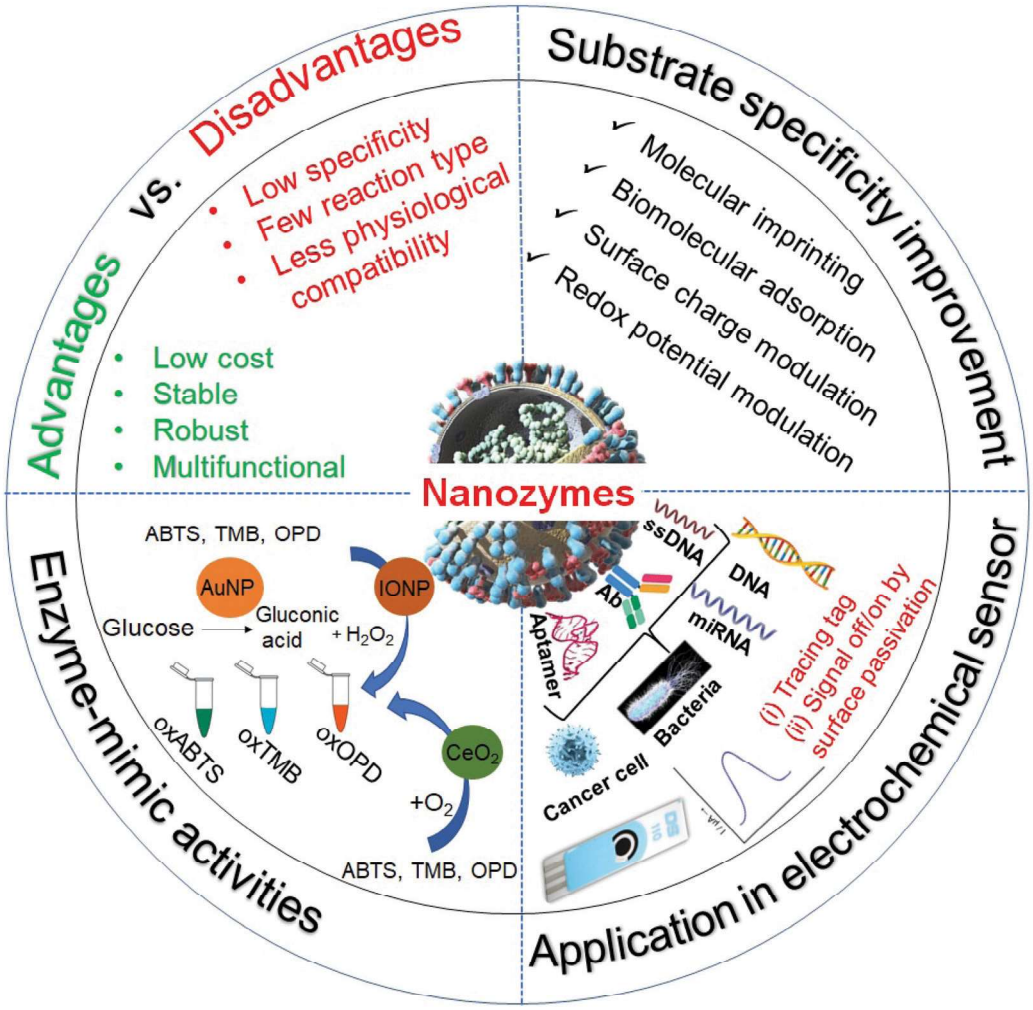

Fig. 1 Schematic presentation of the typical enzyme-mimetic activities of nanozymes, their advantages, and limitations compared to natural enzymes, recommended strategies to improve their substrate specificity, and their applications in electrochemical biosensors.

cent, surface-enhanced Raman scattering, and electrochemical biosensors.[6] The most common nanozymes used in these sensing systems include metal NPs (*e.g.*, Au NPs,[7–9] Pt NPs,[9–13] Pd NPs[9,14]), metal oxide NPs (*e.g.*, CeO_2 NPs, CuO NPs, $BiFeO_3$ NPs, $CoFe_2O_4$ NPs), carbon-based nanomaterials (*e.g.*, carbon nanotubes (CNTs), and graphene oxide (GO)). In general, nanozymes can oxidize a variety of chromogenic substrates (*e.g.*, 3,3′,5,5′-tetramethylbenzidine (TMB), 2,2′-azino-bis(3-ethylbenzthiazoline-6-sulfonic acid) (ABTS), 3,3′-diaminobenzidine (DAB), and *o*-phenylenediamine dihydrochloride (OPD)) in the presence of hydrogen peroxide (H_2O_2) and produce a distinguishable color. This concept has already been proven useful to detect not only H_2O_2 but also other biologically relevant molecules like glucose or lactate when it becomes a part of cascade enzymatic reactions or tandem catalysis by a hybrid nanozyme.

A hybrid nanozyme can be made through assembling either glucose oxidase (GOx) or oxidase-like nanozymes on the surface of iron oxide nanozyme or with other peroxidase mimics.[15–17] In this assembly, oxidase activity is crucial as it provides peroxidase-like nanozyme with hydrogen peroxide to induce a color change or emit light in colorimetric or fluorescent sensors respectively. Integration of two or more nanozymes could improve the catalytic efficiency by enhancing the proximity effect, *i.e.* the first enzymatic reaction occurs in close (nanoscale) proximity to the second enzyme, thereby overcoming the limitation of diffusion-limited kinetics and intermediate instability.[17,18] However, reversible surface passivation of pristine noble metal nanozymes with single-stranded DNA (ssDNA) or an aptamer is an excellent way to develop on/off colorimetric sensors.[19–22] Another intriguing strategy is the use of self-regulated colorimetric sensors that use the nanozyme activity of nanoceria to detect acetylcholinesterase, nerve agents, drugs, and bioactive ions.[23] Several other sensitive colorimetric sensors based on functional nanozymes have also been reported for the detection of biothiols and proteins,[24] point-of-care (POC) testing of cocaine,[25] and lateral flow immunochromatographic analysis of glycoprotein[26] and bacteria.[27]

In electrochemical biosensors, nanozymes can be used in two ways: (i) as an electrode material for biomarker sensing or

(ii) as a tracing tag for signal amplification. As an electrode material, nanozymes have widely been used to fabricate the third and fourth generations of glucose sensors[28] as well as to detect cancer cells.[29,30] High surface area and high density capture sites of the nanozymes could allow enhanced loading of the electroactive species at their surfaces, resulting in improved electrochemical responses. For example, Wang *et al.* used peroxidase-mimicking graphene-supported ferric porphyrin as a tracing tag for signal amplification in detecting DNA.[31] A high loading of porphyrin on both sides of graphene oxide (GO) offered an attomolar-order of sensitivity.

Wei *et al.* published a review on nanozymes in 2013.[32] Since then, numerous review articles have been published on the synthesis, functions, and applications of nanozymes. For instance, Sun *et al.*[33] reviewed carbon-based nanozymes and their applications for the detection of disease biomarkers. Singh *et al.*[34] reviewed the biosensing applications of cerium oxide-based nanozymes. Gao *et al.*[17] discussed the synthesis and applications of Fe_3O_4 and Fe_2O_3 NP-based nanozymes. Biomedical applications of other nanostructured materials as nanozymes have also been covered extensively in the literature.[5,35–42] Very recently, Huang *et al.*[4] and Wu *et al.*[2] discussed the classifications and mechanisms of enzyme-like activities, regulation and control over their activities. They also reviewed the applications of nanozymes in the fields of biomedical and environmental sciences. A recent book has provided an comprehensive overview of materials used for nanozyme synthesis and characterization along with cutting-edge biomedical and environmental applications.[43] However, to the best of our knowledge, no review paper is currently available for nanozyme based electrochemical biosensors for the detection of disease biomarkers.

This review covers the classifications, synthesis methods, and current state-of-the-art development of nanozyme-based electrochemical biosensors. We focus on the applications of nanozyme-based electrochemical biosensors for disease biomarker detection published mostly from 2015 onward. We also highlight the challenges associated with nanozyme-based electrochemical biosensors and provide the possible solutions and strategies to address these limitations.

2. Common nanozymes for electrochemical biosensors

Intense research and investigation have been conducted to reveal the nanozyme activities of various nanostructured materials. Until now, several nanomaterials have been reported to have catalytic activities similar to peroxidase, oxidase, catalase, and superoxide dismutase (SOD). Based on the reaction mechanism, nanozymes can be divided into two main families:[4] (i) the oxidoreductase family and (ii) the hydrolase family. Oxidoreductase nanozymes catalyze the oxidation reaction, where reductants and oxidants work as electron donors and acceptors, respectively. Over the past several years, graphene- and AuNP-based nanozymes have been demonstrated to possess excellent peroxidase-like activity to catalyse the oxidation of many substrates, such as TMB and ABTS in the presence of H_2O_2.[4] It has also been shown that other metallic nanoparticles have oxidoreductase activities. For example, Tremel *et al.* reported that MoO_3 nanoparticles work as nanozymes for the oxidation of SO_3^{2-} to SO_4^{2-} under physiological conditions.[44] On the other hand, hydrolase nanozymes catalyze the hydrolysis reaction by cleaving chemical bonds. In this process, a larger molecule dissociates into two smaller molecules. For instance, gold nanoparticles have widely been used as common hydrolase nanozymes to catalyse hydrolysis reactions.[45–47]

In terms of the free radical scavenging capability, nanozymes can also be categorized as (i) antioxidants and (ii) pro-oxidants.[48] In biological systems, the pro-oxidant induces oxidative stress by producing free radicals. For example, the presence of a transition metal can produce the hydroxyl radical ($HO^{\bullet}$) by the Fenton chemistry.[49] Therefore, certain peroxidase or oxidase involved in the reaction of free radical generation could be regarded as a pro-oxidant.[48] In contrast, antioxidant nanozymes clean up or scavenge free radicals by using catalase- or SOD-like activities.[48] SOD-mimetic catalyzes the dismutation of superoxide anions into hydrogen peroxide, which in turn can be converted to molecular oxygen and water through a catalase-like nanozyme. On the other hand, peroxidase-like nanozyme may convert hydrogen peroxide into a hydroxyl-free radical and oxidize, and produce a colored product. Similar colored products may also be produced by oxidase-like nanozymes through direct oxidation of a chromogenic substrate. Fig. 2 summarizes the classification of nanozymes based on both the reaction mechanism and free radical generation/scavenging.

Among the oxidoreductase nanozymes, peroxidase- and oxidase-mimicking nanomaterials are mostly explored for electrochemical biosensors (Table 1). The common nanomaterials with peroxidase mimetics include metal nanoparticles (AuNPs,[50] PdNPs[51]), metal oxides (Fe_2O_3,[52,53] Au–NPFe_2O_3NCs,[54,55] Fe_3O_4 MNPs,[56] CeO_2/NiO,[57] and CuO[58]), core–shell nanostructures (Au@Pt[59]), dendrites (dealloyed-AuNi@pTBA,[60] Cu–Co alloy dendrites[61]), carbon-based composites (GO-AuNPs,[62] His@AuNCs/rGO,[63] PtNP decorated CNTs[64]), and metal–organic frameworks (MOFs). Unlike other nanomaterials, MOFs have drawn enormous interest as a new class of nanozymes due to their uniform cavities which are likely to provide biomimetic active centers and enzyme-like pseudo-substrate-binding pockets.[65]

3. Synthesis of common nanozymes used in electrochemical biosensors

The peroxidase-like activity of nanozymes is mainly dependent on their surface area to volume ratio (*i.e.*, density of the exposed active sites at the surface of the nanozymes) as well as their affinity towards organic substrates such as TMB and ABTS.[2] The size,[8,90] shape,[91] morphology,[92] compositions, and

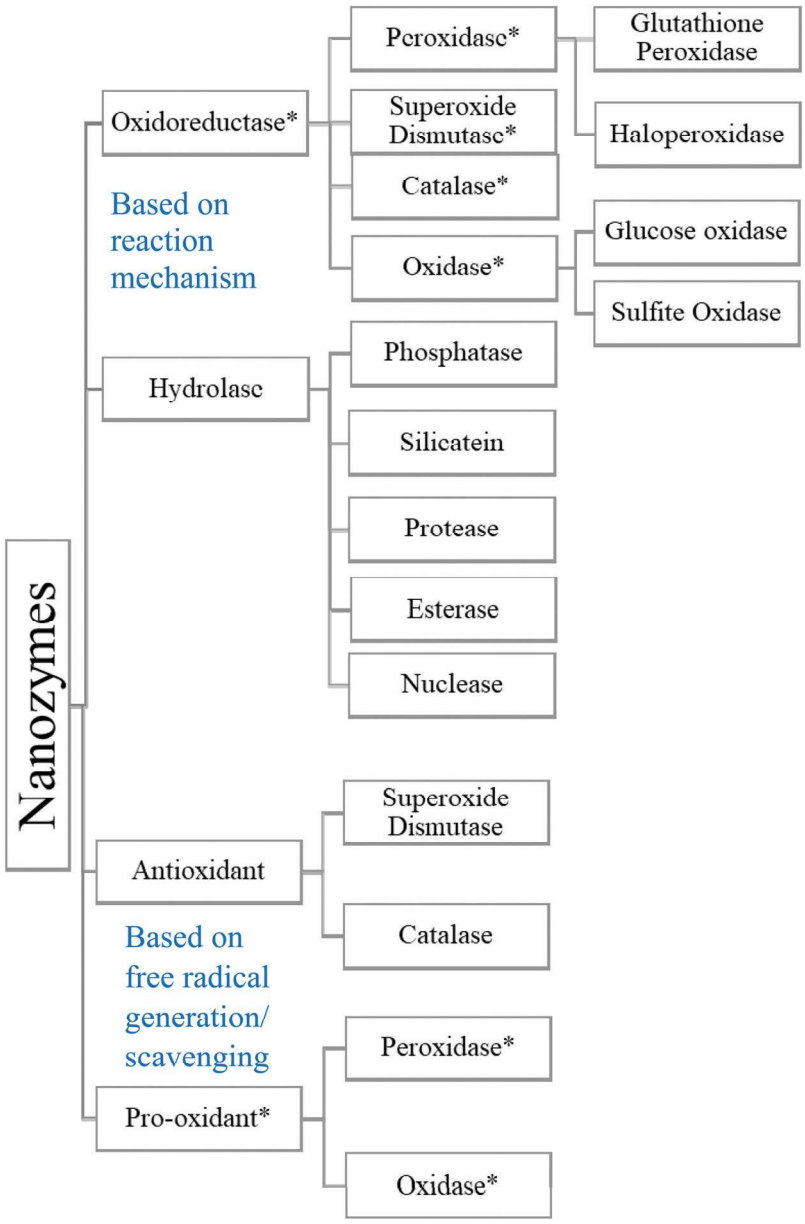

Fig. 2 Classification of nanozymes.[4,48,49] (*) Mark represents the nanozymes commonly used for electrochemical biosensors.

surface modification groups[93,94] of nanozymes can also influence their peroxidase-like activities. It is important to note that the size, shape, composition and morphology of the nanostructured materials can be controlled by changing the reaction parameters,[95,96] precursor amount and volume[97,98] and selecting appropriate synthetic methods.[3]

Due to the potential applications of nanozymes in electronics,[99] therapeutics, optics,[100] catalysis[101] and biosensing[102] applications, there has been a demand for the design and synthesis of nanozymes with high peroxidase-like activities. Over the past few years, many attempts have been made to synthesize nanozymes with well-controlled size, shape, spatial arrangement, and compositions. These methods can be divided into two main categories: top-down and bottom-up approaches. The top-down approach is the solid-state processing of macroscopic materials to nanophasic products. This approach includes mechanical milling, nanolithography, laser ablation, sputtering and thermal decomposition. However, the top-down approach is not suitable to make a well-controlled size and shape and may produce many crystallographic defects in the nanostructure. In contrast, the bottom-up method follows building up of nanostructures through the atom-by-atom or cluster-by-cluster or molecule-by-molecule approach. It offers nanomaterials with a uniform size, shape, fewer defects and homogeneous chemical compositions. The bottom-up approach mostly includes processes such as sol–gel, reverse micelle, chemical vaour deposition (CVD), pyrolysis, biosynthesis, microwave-assisted, and flow synthesis, and

Table 1 Nanozymes used in electrochemical sensors for biomarker detection

Nanozyme	Function	Substrate	Target	LOD	Ref.
$CoFe_2O_4$ MNPs	A nanoelectrocatalyst for toluidine blue catalysis	Toluidine blue	microRNA (*i.e.*, microRNA-21)	0.3 fM	66
PdNPs@Fe-MOFs	Tracer indicator	TMB + H_2O_2	microRNA(*i.e.*, microR-122)	0.003 fM	67
Fe_3O_4 and Cu(II) complex	Fe_3O_4NPs acts as a magnetic nanocarrier. Increase of sensitivity because of the synergistic effect of the Fe_3O_4 nanozyme and Cu (II) complex.	TMB + H_2O_2	microRNA (microR-21)	33 aM	68
FeTCPP@MOF composites	Increased diffusion of *o*-PD permitted by the porous structure of the nanozyme	*o*-PD + H_2O_2	DNA	0.48 fM	69
Au@PtNPs	Used as a trace tag	PNP + $NaBH_4$	DNA	0.3 aM	70
ZrHCF MNPs	DNA can be bound to ZrHCF MNPs through the interaction from the phosphate group from DNA and Zr(IV) from ZrHCF without chemical modification.	H_2O_2	DNA	0.43 fM	71
Hemin/G-quadruplex DNAzyme	—	TMB + H_2O_2	HBV DNA	0.5 pM	72
Mesoporous iron oxide (MIO)	MIO functionalized with 5mC antibody recognizes 5mC immobilized on SPGE	TMB + H_2O_2	Global DNA methylation (5mC)	10% of methylation in genomic DNA	53
Au@NPFe_2O_3NC	Nanocarriers for target p53 from serum	TMB + H_2O_2	p53 autoantibodies	0.02 U mL^{-1}	73
Au–NPFe_2O_3NC	Direct isolation of the target protein from serum	TMB + H_2O_2	p53 autoantibody	0.08 U mL^{-1}	54
Fe_3O_4/Au@Pt	Used as a nanocarrier for natural HRP, DNAzymes and aptamer. Co-catalysis for signal enhancement	Hydroquinone (HQ) + H_2O_2	Cardiac troponin I (cTnI)	7.5 pg mL^{-1}	74
Fe_3O_4@UiO-66/Cu@Au	Formation of cluster-based nanoprobes for further enhancing the detection sensitivity	HQ + H_2O_2	Cardiac troponin I (cTnI)	16 pg mL^{-1}	75
Mn_3O_4/Pd@Pt	Used for nanoprobe formation which will increase further sensitivity through loading with HRP.	HQ + H_2O_2	HER2	0.08 ng mL^{-1}	76
Pt–Cu HTBNFs	Bind to the target through the anchored detection antibody and act as a signal enhancer.	H_2O_2	PSA	0.03 pg mL^{-1}	77
Au@ZIF-8(NiPd)	Thrombin binding aptamer anchored Au@ZIF-8(NiPd) acts as a signaling probe.	H_2O_2	Thrombin (TB)	15 fM	78
Au@MGN (gold-magnetic graphene nanocomposite)	Antibody functionalized Au@MGN forms a sandwich	H_2O_2	Tissue polypeptide antigen	7.5 fg mL^{-1}	79
Pt@P-MOF(Fe)	A catalyst and redox mediator to detect the telomerase activity.	H_2O_2	Telomerase activity	Telomerase activity from 20 HeLa cells per mL	80
Au–NPFe_2O_3NC	Tetraspanin functionalized nanocubes were used as a dispersible capture agent for bulk exosomes	TMB + H_2O_2	Exosome	10^3 exosomes per mL	55
CuO/WO_3-GO	Folic acid-modified CuO/WO_3-GO capture cancer cells by recognizing the folate receptor results in signal attenuation.	OPD + H_2O_2	Cancer cells	18 cells per mL	29
NGQD@NC@Pd HNS	Electrocatalytic reduction of H_2O_2 released by cancer cells.	H_2O_2	Cancer cells	—	81
CuO	The MUC-1 aptamer modified CuO nanozyme was used for selective binding to MCF-7 CTCs and catalyzing the reduction of H_2O_2 for higher sensitivity	H_2O_2	CTCs	27 cells per mL	58
rGO/MoS_2 composites with Fe_3O_4NP bienzyme	Immunomagnetic beads (Fe_3O_4NPs) help in the enrichment of CTCs. The synergistic peroxidase activity of rGO/MoS_2 and Fe_3O_4NPs for signal amplification	TMB + H_2O_2	CTCs	6 cells per mL	82
Graphene Quantum Dots (GQD)	—	H_2O_2	*Yersinia enterocolitica*	5 CFU mL^{-1} (milk), 30 CFU mL^{-1} (human serum)	83
Gold nanoparticles (GNPs)	The F23 aptamer leaves GNPs after interacting with *Pseudomonas aeruginosa* which ensures the revival of the peroxidase activity of GNPs	TMB	*Pseudomonas aeruginosa*	60 CFU mL^{-1}	50
$Co_3(PO_4)_2$ NRs	Used as electrode materials	Superoxide anion ($O_2^{\bullet-}$)	$O_2^{\bullet-}$ released from cancer cells	2.25 nM	84

Table 1 *(Contd.)*

Nanozyme	Function	Substrate	Target	LOD	Ref.
Mn-MPSA-HCS and Mn-MPSA-HCC	Used as electrode materials	Superoxide anion ($O_2^{\bullet-}$)	$O_2^{\bullet-}$ released from cancer cells	1.25 nM	85
GS@ZIF-67	Used as electrode materials	Electrocatalytic oxidation of glucose	Glucose	0.36 μM	86
Poly acrylic acid-coated nanoceria (PNC)	PNC catalyses TMB in the absence H_2O_2	TMB	Norepinephrine	66 nM	87
h-CuS NCs	—	TMB + H_2O_2	Glucose	—	88
Au/Co@HNCF	—	UA	UA	0.023 μM	89

most of these processes refer to as wet chemical synthesis.[103–105] In the following sections, we highlight the synthesis of metal oxide, metallic and carbon-based nanozymes with different sizes, shapes and morphologies using top-down and bottom-up approaches.

3.1 Synthesis of metal oxide nanozymes

Thermal decomposition (also called thermolysis) is a process where chemical bonds of a compound are subjected to dissociation through thermal energy resulting in the formation of monodispersed nanoparticles in a single step. Usually, an organometallic precursor is heated in a high-boiling point organic solvent in the presence of a suitable surfactant, such as oleic acid, 1-octadecene, 1-tetradecene or oleylamine. As an early attempt to synthesize monodispersed iron oxide nanocrystals, Park *et al.* slowly heated an iron–oleate complex in 1-octadecene at different temperatures. They observed that the temperature dependence of nucleation and growth kinetics was instrumental in the monodisperse nanocrystal formation. They also reported that metal oxide NPs (*i.e.*, Fe_2O_3, CoO, MnO, FeO@Fe, and $MnFe_2O_4$) with different sizes could be synthesized by using organic solvents with high boiling points, namely 1-hexadecene and trioctylamine (*i.e.*, these solvents have the boiling point of 274 °C and 365 °C respectively). The high yield (>95%) and large scale production (40 g) are two characteristic features that have made this process state-of-the-art for nanocrystal synthesis.[104] Another study also supported that high temperature synthesis leads to the increase of the nanoparticle size due to the comparatively higher reactivity of the metal complex in the solvent.[106] However, the metal oxide NPs with nanozyme activity prepared by this method are usually smaller in size, crystalline and dispersed only in an organic solvent.

The sol–gel process for metal oxide synthesis is a wet chemistry based technique, which is accomplished at room temperature. This method is comparatively cheaper than other wet chemical methods. In this method, a sol is a stable dispersion of colloidal particles or polymers in a solvent, and a gel consists of a three-dimensional continuous network, which encloses a liquid phase. The sol–gel method involves hydrolysis and condensation of metal alkoxides, leading to the dispersion of metal oxide particles in a sol, followed by drying or gelling through solvent removal or by using a chemical reaction. This method consists of several steps, namely hydrolysis, condensation, drying, and thermal treatment to realize the final product of metal oxide NPs.[107–111]

Solvothermal and hydrothermal synthesis methods are other well-established wet chemical methods to produce metal–oxide NPs. These methods are carried out in an autoclave or a Parr bomb at high temperature (100 to 1000 °C) and high pressure (1 to 10 000 bar). The main difference between hydrothermal and solvothermal methods is that water is used as a precursor solvent for hydrothermal synthesis, whereas organic solvents are used in solvothermal synthesis. These methods do not require a protective gas atmosphere and refluxing conditions and are more convenient compared to the coprecipitation and thermal decomposition methods. Metal oxide NPs obtained in these methods are highly pure, selective, reproducible and crystalline. Moreover, the crystalline characteristic of the NPs can be altered by the total reaction time. For instance, it was reported that the transformation of hydrothermally produced airon oxide nanozymes from a 0D to 3D structure is time-dependent.[103] Li *et al.* applied a solvothermal reaction to synthesize metal-ion-doped (such as Sn^{4+}, Fe^{3+}, Co^{2+}, and Ni^{2+}) TiO_2 nanocomposites. The size and shape of the TiO_2NPs were controlled by using lauryl alcohol both as a solvent and surfactant for the reaction.[112]

The microwave-assisted chemical synthesis process is an alternative wet chemical technique for the synthesis of metal oxides NP based nanozymes. Recent evidence suggests that this method produced NPs with a uniform size and ultrafine shape. In a conventional heating system, it is quite impossible to transfer the heat uniformly to the reactant precursor. In contrast, microwave-assisted synthesis provides uniform heating and thus reduces the reaction time by increasing the reaction kinetics. This method is safe and convenient and requires less energy for the completion of the reaction because of its fast nucleation and growth rate. Recently, several metal-oxide based nanozymes have been synthesized by using the microwave-assisted method. These include ZnO,[113] α-Fe_2O_3, β-Fe_2O_3, Fe_3O_4,[114] CuO,[115] Cu_2O,[116] Mn_3O_4, MnO_2,[117] TiO_2,[118] and Co_3O_4.[119] It is important to note that the phase and shape of the NPs can be altered by the properties of solvents used in the method. Guru *et al.* have shown that the synthesis of iron oxide NPs by the microwave-assisted method could be drastically affected by using different glycols.[120] Three different glycols (ethylene glycol, polyethene glycol and polypropylene glycol) with the same precursor under the same conditions

resulted in three NPs with different phases (Fe_3O_4, α-Fe_2O3, and γ-Fe_2O_3) and shapes (35, 29.9 and 28.2 nm).

3.2 Synthesis of metallic nanozymes

Metallic NPs are synthesized by a range of physical processes, chemical reductions, and biological methods. The commonly used physical processes for the synthesis of metallic NPs include grinding, UV irradiation, microwave irradiation, and laser ablation methods. Chemical reduction is the most widely used technique where metal salts are reduced in the presence of a suitable reducing agent.[121,122] Citrate has been used as a reducing agent for chloroauric acid and silver nitrate to synthesize AuNPs and AgNPs, respectively.[123,124] Metallic NPs produced by this method have a high tendency to aggregate. To stop this tendency, stabilizing agents, such as polyvinyl alcohol, poly(vinylpyrrolidone), bovine serum albumin (BSA), citrate and cellulose, are mostly used in the reduction reactions. The size of the NPs can be tuned by changing the ratio of the stabilizing agent and the metal salt.[125] In biological methods, non-toxic and inexpensive microbes are used to produce a variety of metallic NPs with different sizes, shapes and compositions. In summary, biological methods are environmentally friendly, whereas chemical reduction methods are hazardous and physical processes suffer from high energy input.

3.3 Synthesis of carbon-based nanozymes

In this section, the synthesis of graphene oxide, CNTs, and carbon nanodot based nanozymes is discussed. Graphene oxide (GO) is a nonconductive and hydrophilic carbon nanomaterial. In general, the synthesis of GO from graphite is a two-step process.[126,127] In the first step, graphite flakes are oxidized to graphite oxide to have oxygen-containing functional groups (*e.g.*, epoxy (C–O–C), hydroxyl (OH), carbonyl (C═O) and carboxyl (R–COOH)) into the basal plane or edge of the graphene sheet. As a result of the oxygen-containing groups, the interlayer distance in GO expands and makes the atomic-thick layers hydrophilic as well. In the second step, oxidized layers can be subjected to exfoliation under moderate sonication, resulting in the release of GO. In 1859, Brodie first synthesized GO by adding potassium chlorate to a slurry of graphite in the presence of fuming nitric acid.[128] This process needs 3 to 4 days to be completed. In 1898, Staudenmaier improved Brodie's protocol by adding concentrated sulfuric acid and fuming nitric acid followed by the addition of chlorate in the reaction mixture. This method produces highly oxidized GO. However, these two processes require a long reaction time. The most widely used Hummers' method,[129] reported in 1958, avoids this disadvantage where high-quality GO can be produced within 2 h. In this method, graphite is oxidized with $KMnO_4$ and $NaNO_3$ in concentrated H_2SO_4. Notably, all three methods produce toxic gas(es): ClO_2 (g) and/or NO_x (g), the former one is explosive. Later, Tour improved the Hummers' method by replacing $NaNO_3$ with the mixture of $9H_2SO_4 : H_3PO_4$. The reaction mixture was fortified with a doubled amount of $KMnO_4$ as compared to the Hummers' method. This method does not produce any toxic gas and generates oxidized GO with a more regular carbon framework and a larger sheet size.[126,130–132] Over the past several years, GO has widely been used to synthesize different hybrid nanostructured materials to produce a range of GO-based nanozymes. For example, Ruan *et al.* synthesized GO/Fe-MOF nanozymes *via* mixing the negatively charged GO with the positively charged Fe-MOF. Electrostatic interactions between GO and Fe-MOF hold them together.[133] A similar phenomenon occurs in the synthesis of GO–AuNP nanozymes. During the aging step of the synthesis, gold ions were adsorbed on the surface of the GO. This step was followed by a reduction reaction with sodium citrate, resulting in the formation of AuNPs onto GO (*i.e.*, GO–AuNP hybrid).[62]

There are various methods for the synthesis, purifications, dispersion, and functionalisation of CNTs.[134] These materials offer enormous benefits in real world applications. In particular, they are attractive for use in bimolecular sensors for environmental and health monitoring.[135] Recent evidence suggests that CNT based materials possess excellent peroxidase-like activities.[136] Qu *et al.* synthesised oxygenated-group-enriched carbon nanotubes (o-CNTs) *via* a one-pot oxidation reflux method.[137] The o-CNTs exhibited enhanced peroxidase-like activity for the catalytic reaction over a broad pH range. They were used to catalyse the formation of the hydroxyl radical, killing bacteria efficiently and protecting the tissue against edema and inflammation induced by bacterial infections. Among other CNT based materials, single-walled carbon nanotubes (SWCNT) and multi-walled carbon nanotubes (MWCNT) have widely been used to fabricate metal nanoparticle (Fe_3O_4, ZnO) or GO based hybrid nanozymes.[138–141] Compared with their single component, these hybrid materials offered enhanced peroxidase-like activities, presumably resulting from the synergetic effects of metallic nanoparticles or GO and conducting CNTs (*i.e.*, SWCNTs or MWCNTs). Recently, it has been shown that Fe_3O_4 nanoparticles loaded on GO-dispersed CNTs show a stronger enzyme-like activity.[140] To synthesize this hybrid material, amphiphilic GO nanosheets could be employed as a "surfactant" to disperse CNTs to create stable GO-dispersed CNT supports in water for covalently loading cubic Fe_3O_4 nanoparticles. Compared with the original Fe_3O_4 and CNT-loaded Fe_3O_4 nanoparticles, the GO/CNT–Fe_3O_4 particles offered enhanced peroxidase-like activities. Similarly, iron containing hemin assembled with SWCNTs showed enhanced peroxidase-like activity.[142] Hemin could be assembled on the surface of SWCNTs through non-covalent functionalization by π–π stacking, and resulted in much higher peroxidase-like activity than the activity of hemin alone.

Carbon nanodots (CDs) or carbon quantum dots (CQDs) are a novel class of carbon nanomaterials with a size less than 10 nm but can be as small as 1 nm. These materials have commonly been synthesized by using top-down and bottom-up approaches.[143–147] Each approach has its own advantages and disadvantages. Top-down approaches are widely used for the synthesis of CDs due to the adequate amount of the raw material, scaled-up production and smooth operation. On the

other hand, bottom-up approaches give attractive opportunities to control the particle size, shape, and properties. Recently, green synthesis of CDs has become more popular than the conventional hydrothermal, solvothermal, electrochemical, and electron-beam lithography methods that usually require toxic chemicals and a large amount of heat energy.[144,146,147] In green synthesis, the organic precursor is replaced by biomass materials and does not require external energy supply.[147] It has been shown that CDs, CDQ, doped CD/graphene QDs, and CD/graphene QD nanocomposites possess peroxidase-like activity.[146] The design, catalytic process, property study, and biosensing application of these materials have also been discussed in the literature.[143–147] These materials have been used in developing biomolecular sensors for the detection of many biologically and environmentally significant targets including glutathione,[148] glucose,[149] and mercury ions.[150]

4. Nanozyme as a substitute of HRP

The enzyme-linked immunosorbent assay (ELISA) is the most routinely used technique for detecting and quantifying peptides and antigens. In ELISA, an enzyme-linked primary antibody (direct ELISA) or secondary antibody (indirect or sandwich ELISA) specifically recognizes an antigen. Until now, HRP is the most widely used enzyme reporter in ELISA. It catalyzes the oxidation of TMB in the presence of H_2O_2 to produce a colorimetric signal, and the intensity of the signal is proportional to the recognized antigen concentration. Despite having many advantages including a high substrate turnover, small size, and facile conjugation ability with other biological receptors, HRP suffers from several drawbacks. The major drawback associated with HRP is its low tolerance to many preservatives such as sodium azide that inactivates the peroxidase activity even at low concentration. It also undergoes proteolytic degradation, and its enzymatic activity is limited to a narrow range of pH and temperature.[5] Moreover, conventional ELISA lacks sensitivity to detect ultra-low concentrations of biomolecules, especially in the early stages of diseases.[151] To overcome these limitations, numerous nanostructured material based nanozymes including MOF based hybrid nanozymes (described above) have been developed, which are believed to be direct surrogates of HRP.[42] For instance, Ruan *et al.* reported the third generation of 2D GO/Fe-MOF hybrid nanozymes, named the nanozyme nest, which was used in a conventional sandwich ELISA to detect the benzo[*a*]pyrene-7,8-diol 9,10-epoxide–DNA adduct (BPDE–DNA), a woodsmoke biomarker found in the blood.[133] This method showed enhanced sensitivity for the oxidation of TMB by the dual peroxidase active nanozyme nest (Fe-MOF and GO). The value of the Michaelis–Menten constant, K_m, (0.3599 mM for the nanozyme nest *vs.* 0.4072 mM for HRP) clearly revealed that the nanozyme nest offers higher TMB affinity than that of HRP. Importantly, this hybrid nanozyme reports a lower LOD value in comparison to that of HRP, suggesting the better sensitivity of the nanozyme nest over HRP in detecting biomolecules.[133]

The peroxidase-like activity of nanozymes can be increased *via* rational design of nanostructured materials as multifunctional nanozymes. Heteroatom doping and the sequence of doping are two effective ways to increase the peroxidase-like activity and specificity of nanozymes. For instance, up to a 100-fold increase in catalytic activity has been reported for nitrogen-doped (N-doped) reduced graphene oxide (N-rGO) nanozymes compared to reduced graphene oxide (rGO) alone.[152] Density functional theory (DFT) calculation revealed that N-rGO selectively activates H_2O_2 over O_2 and $^{\bullet}O_2^-$ and forms stable radical oxygen species adjacent to N-doped sites. These radical oxygen species, in turn, oxidize peroxidase substrates (*e.g.*, TMB) and offer enhanced responses. In another study, Kim *et al.* showed a 1000-fold higher catalytic efficacy (k_{cat}/K_m) of N and B co-doped reduced graphene oxide (NB-rGO) compared to that of rGO alone. The catalytic performance of this material is very similar to that of the natural HRP. They have also demonstrated that the sequence of doping of heteroatoms in the nanostructure materials could significantly affect the catalytic efficacy (k_{cat}/K_m) of nanozymes. For example, the catalytic activity of BN-rGO resulted in a ~30% lower k_{cat} compared to that of NB-rGO.[150] A high surface to volume ratio, and π–π and hydrophobic interactions assist NB-rGO to acquire stronger affinity towards substrates (*e.g.*, TMB) than that of HRP. Due to this property, NB-rGO nanozymes were able to detect C-reactive protein (CRP), a reliable biomarker of inflammation, tissue damage and cardiovascular disease, *via* the oxidation-dependent rapid color change of TMB within 3 minutes. In contrast, HRP-based ELISA needs at least 10 minutes. It also shows a three-times lower LOD (~5 ng mL^{-1} of CRP) than that of HRP.[150]

5. Applications of nanozymes in non-electrochemical assays

5.1 Lateral-flow immunodetection

The lateral-flow immunostrip (*i.e.*, nanozyme-strip), a paper-based biosensor, is considered as one of the excellent demonstrations for POC testing of biomolecular targets because of its operational simplicity, rapid analysis, naked-eye detection and low cost. Generally, lateral flow biosensors are composed of a sample pad, a conjugate pad, a nitrocellulose membrane containing test and control lines, and an absorbent pad. Many nanozymes have been integrated into this form of the assay. For example, Duan *et al.* reported a Fe_3O_4 magnetic nanoparticle (MNP) based immunochromatographic strip to detect the glycoprotein of ebolavirus (EBOV).[26] In this assay, the MNP conjugated detection antibody (anti-EBOV) recognizes EBOV, which in turn forms a sandwich complex with the capture antibody in the test line. After the formation of the immunocomplex, oxidation of the peroxidase substrate develops color for visual observation, indicating the presence of EBOV. Pre-processing the sample with immunomagnetic separation offered

an additional sensitivity to the EBOV analysis. Overall, this strip demonstrates a 100-fold higher sensitivity over the standard colloidal AuNP based strip with the LOD of 1 ng mL^{-1} of glycoprotein (≈240 pfu ml^{-1}). This method requires less than half an hour[26] and it is sensitive enough to detect Ebola at the onset of symptoms.

Recently, a porous platinum core–shell nanocatalyst (PtNCs) based immunostrip has been developed to detect the p24 HIV capsid protein, a reliable marker for HIV diagnosis (Fig. 3). In this assay, both target specific antibody-functionalised PtNCs and orthogonally biotinylated camelid antibody fragments (nanobody-biotin) are designed to recognize the distinct regions of the target p24 protein.[153] In the presence of the test sample (*i.e.*, serum or plasma contacting p24 protein), p24 protein-bound PtNCs become biotinylated through complexation with the biotinylated nanobody fragments. At the polystreptavidin-coated test line, rapid high affinity biotin–streptavidin binding enables a target dependent deposition of the biotinylated p24 protein-bound PtNC complex. PtNCs bound at the test line catalyze the oxidation of the 4-chloro-1-naphthol/3,3′-diaminobenzidine tetrahydrochloride (CN/DAB) substrate in the presence of H_2O_2 producing an insoluble black product which is clearly visible with the naked eye. This method allows the detection of acute-phase HIV in clinical human plasma samples in 20 min.

5.2. Colorimetric sensor

Colorimetric detection of an analyte has the advantage of providing a fast response (color change) to obtain visual observation (naked eye) and subsequent UV-visible quantification.

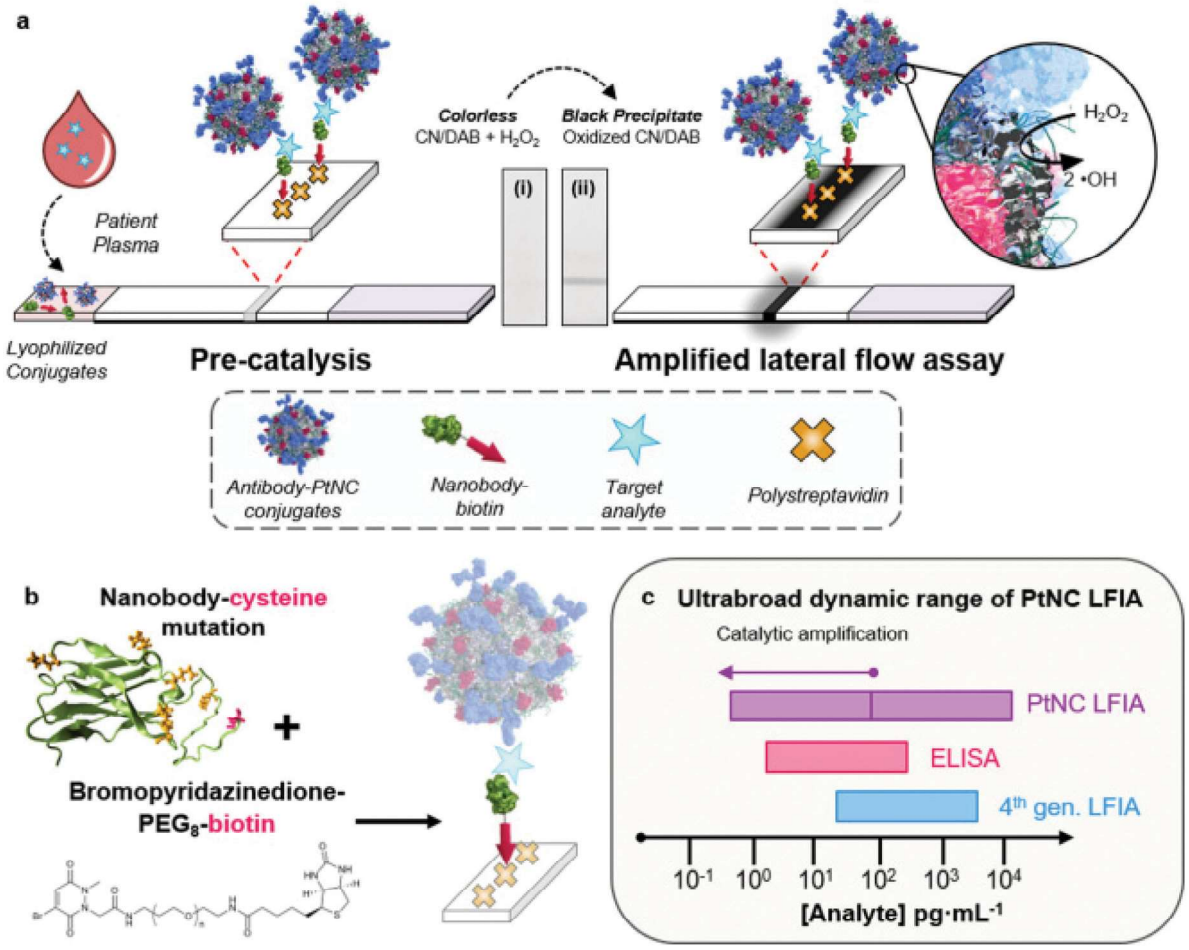

Fig. 3 (a) Schematic representation of paper based lateral flow immunoassays (LIFA). Antibody functionalized Pt nanocatalysts (PtNCs) and biotinylated nanobody fragments are mixed with the test samples (*i.e.*, plasma or serum). If the test samples contain the target p24 capsid protein, it sandwiched between the antibody–PtNC and biotinylated nanobody fragment, forming a biotinylated complex. A lateral flow strip, composed of a nitrocellulose reaction membrane and an absorbent pad, is used to draw this complex up the strip toward a streptavidin-modified test line by capillary action. At the test line, the peroxidase-like activity of PtNCs is used to catalyze the oxidation of the CN/DAB substrate in the presence of H_2O_2 producing an insoluble black product (*i.e.*, naked-eye observation). (b) Site-selective chemical modification of a nanobody with an exposed cysteine mutation (red), where lysine residues are highlighted in orange on the structural model (left), and the cartoon of oriented elements at the streptavidin test line. (c) Comparison of dynamic ranges of 4th generation LIFA, ELISA and PtNC LIFA. Reprinted with permission from Ref (154) (https://pubs.acs.org/doi/abs/10.1021/acsnano.7b06229). Copyright (2018) American Chemical Society. Further permissions related to the material excerpted should be directed to the American Chemical Society.

An advantage of naked-eye detection is that it can be employed as a first-pass screening test for rapid diagnosis of diseases. Once positive results are obtained, UV-vis or other quantity measurements (*i.e.*, electrochemical detection) could be performed to quantify the level and severity of diseases to determine the treatment options, a management strategy, which could significantly reduce the cost and time associated with the disease diagnosis and management. This feature of colorimetric sensors makes it suitable for developing rapid and inexpensive screening tools in the fields of medicine (*i.e.*, detection of disease-specific molecules, proteins, and cells), biotechnology, and environmental sciences. As a peroxidase mimicking nanozyme can oxidise chromogenic substrates (*e.g.*, TMB, ABTS, and OPD) and produce a color in the presence of H_2O_2, it can directly detect H_2O_2 or other H_2O_2 producing substrates (*e.g.*, glucose).

The peroxidase-like activity of both the iron oxide nanocomposites (*e.g.*, PDDA coated Fe_3O_4 MNPs,[154] mesoporous silica encapsulated Fe_3O_4 MNPs,[155] Fe_3O_4-GO composites,[156] CeO_2-coated hollow Fe_3O_4 nanocomposites[157]) and iron-containing nanomaterials (*e.g.*, assembling hemin in ZIF-8[18]) have widely been used for glucose detection. In all the cases, these materials were combined with GOx and the synergistic effect of these two enzymes was the key factor in achieving high sensitivity and superior analytical performance in biomolecular sensing. Again, the sensitivity of glucose detection can also be increased by introducing pores to iron oxide nanoparticles as it increases the effective catalytic surface area and exposes the metal ions to the surface. For instance, Masud *et al.* detected a glucose concentration as low as 0.9 μM with the mesoporous iron oxide (γ-Fe_2O_3), which is ten-times more sensitive than that of the assay with ZIF-8 (NiPd) nanoflowers.[158] In addition to porosity, the oxidation state of the metal could also influence the nanozyme activity. The $LaNiO_3$ perovskite with Ni^{3+} demonstrated a 58-fold and 22-fold higher peroxidase activity than that of a perovskite with Ni^{2+} (*e.g.*, NiO nanoparticles) and N^0 (*e.g.*, Ni nanoparticles) oxidation states, respectively. In addition to porosity, the oxidation state could influence the activity of nanozymes. A $LaNiO_3$ perovskite with Ni^{3+} demonstrated a 58-fold and 22-fold higher peroxidase activity than that of nanoparticles with Ni^{2+} (*e.g.*, NiO nanoparticles) and N^0 (*e.g.*, Ni nanoparticles) oxidation states, respectively. The superior activity of these nanozymes facilitated the colorimetric assays of H_2O_2, glucose, and sarcosine.[159] However, as described by Wang *et al.*, the occupancy of the e_g orbitals of the central metal ions may affect the peroxidase-like activity of the perovskite nanozyme.[160]

In recent years, nanozymes have also been used in the colorimetric detection of DNA methylation,[161] a potential epigenetic biomarker. Shiddiky's group has developed a unique method for detecting DNA methylation using the peroxidase-like activity of the mesoporous iron oxides.[53] In this assay, the target DNA samples were extracted and denatured prior to their adsorption onto the surface of a bare screen-printed gold electrode (SPGE) *via* the gold–DNA affinity interaction. 5-Methyl cytosine antibody (5mC) functionalized mesoporous iron oxide nanozymes were then used to recognise the methyl cytosine groups present on the SPGE. The nanozymes catalyze the TMB in the presence of H_2O_2 to give the colorimetric (*i.e.*, naked-eye observation) and electrochemical quantification of the methylation level. The assay could successfully detect as low as 10% difference of global DNA methylation level in synthetic samples and cell lines with good reproducibility and specificity (% RSD = <5%, for $n = 3$).

Modulation of the peroxidase-like activity of nanozymes *via* interacting with molecules and ions present in biological systems can be used to detect biomolecular targets. Shah *et al.* used the interaction of AuNP nanozymes with ATP, ADP, carbonate, sulphate and phosphate ions and the resultant peroxidase-like activity was calculated.[162] It was shown that compared to ADP, phosphate, sulphate and carbonate ions, the incorporation of ATP in the system could significantly enhance the nanozyme activity of AuNP nanozymes. In contrast, surface passivation of citrate-capped AuNPs with the DNA aptamer inhibits the peroxidase substrate to reach the AuNP surface, thereby attenuating their nanozyme activity. However, when the aptamer binds to its specific targets, it leaves the AuNP surface and reactivates the nanozyme activity. Based on this phenomenon, Weerathunge *et al.* used a AuNP–aptamer transducer to detect murine norovirus with a detection limit of 3 viruses (~30 viruses per mL) within 10 min.[21] As the method can be used for other aptamers (*i.e.*, it is not limited to any specific aptamers), this AuNP nanozyme-based sensor can be adopted for the detection of other viruses.

5.3 Fluorescence sensor

A fluorescence sensor consists of the emission of light by a material (fluorophore) after being excited at lower wavelengths and the intensity (or lifetime) of that emission varies with the concentration of the target analyte.[163] In this type of sensor, the nanozyme converts a non-fluorescent substrate into a fluorescently active one by catalysing the hydrolysis or oxidation reaction. For instance, it was reported that iron and nitrogen-incorporated CNTs that were grown *in situ* on 3D porous carbon foam (denoted as Fe-Phen-CFs) possess a peroxidase-like activity, which could oxidise terephthalic acid (TA) to the fluorescent product of hydroxyl terephthalate (HTA) in the presence of H_2O_2 and can be used as a unique strategy for fluorescence detection of H_2O_2.[164] However, similar to other peroxidase-mimicking nanozymes, Fe-Phen-CFs need to be coupled with GOx. The method showed excellent sensitivity towards the detection of H_2O_2 and glucose with a detection limit of 68 nM and 0.19 mM, respectively.

In recent years, a ratiometric fluorescence sensor has gained popularity because of its built-in self-calibration for signal correction, enabling more reliable detection. It also enables more accurate imaging contrast, which often leads to higher detection sensitivity. Ratiometric fluorescence sensors can effectively overcome most of the issues associated with false positive results in traditional fluorescence sensing by introducing another fluorescence emission band to achieve ratiometric signal readouts.[165,166] Very recently, this sensor

has been used for the detection of H_2O_2 and glucose. Briefly, the peroxidase-like activity of ruthenium ion/carbon nitride (Ru–C_3N_4) nanosheets catalyse OPD to fluorescent DAB which exhibits emission at 565 nm. Meanwhile, fluorescence emission at 455 nm by Ru-C_3N_4 decreases or quenches due to the inner filter effect of the generated DAB. *Via* this method, an excellent sensitivity and selectivity to serum glucose in the presence of common interferents were obtained.[166]

6. Applications of nanozyme-based electrochemical biosensors

An electrochemical biosensor provides a suitable platform that facilitates the formation of a probe–target complex (*i.e.*, a specific recognition event) in such a way that the binding event triggers a useable signal for electrochemical readout.[167] Over the past several decades, electrochemical biosensors have successfully been used in detecting a range of molecular and cellular biomarkers in the fields of biomedical, biotechnology, and environmental sciences. Most importantly, the electrochemical detection system is amenable to miniaturization and offers other advantages such as simplicity, cost-effective nature, and high sensitivity and specificity.[168] As shown in Fig. 4, biorecognition and signal transduction are two critical elements in the fabrication of electrochemical biosensors, and nanozymes have played an essential role in this regard.

6.1 Genosensor

Detection of specific nucleic acid (DNA or RNA) sequences has proved their utility in molecular diagnostics, pathogen detection and nanomedicine (nanoscience and nanotechnology) applications in life and health sciences. It is known that many malignant diseases (*e.g.*, cancer) and pathogenic infections present their signature nucleic acid markers (*e.g.*, circulating tumor DNA, microRNA) in the peripheral circulatory system which can be used as diagnostics, prognostics and therapeutic markers.[169,170] The concentration of these circulating biomarkers in the peripheral blood or other bodily fluids (saliva, urine, *etc.*) is extremely low at the early stages of diseases.[170] Therefore, highly sensitive and specific analysis/detection methods are required. To achieve this goal, the nanozyme-based catalytic signal amplification strategy for nucleic acid detection is one of the promising options.

In electrochemical nucleic acid biosensors, the sensitivity can easily be enhanced *via* incorporating a catalytic hairpin assembly (CHA) combined with nanozyme label-based redox cycling signal amplification. As outlined by Hun *et al.*, CHA was used to form a double stranded DNA on a AuNP modified electrode.[70] Initially, hairpin H1 was immobilized onto AuNP modified gold electrodes and in the presence of the target DNA, the stem–loop structure of H1 opened due to binding to the target DNA and formed a double strand product with 21 base hybridization. This triggered the opening of the second hairpin and formed partially complementary dsDNA with 39 base hybridization. This step released the target DNA which could be recycled and used for opening another H1. In the second step, a DNA probe functionalized Au@PtNP nanocatalyst was hybridized with the electrode attached DNA. Au@PtNPs can catalyze the reduction of *p*-nitrophenol (PNP) to *p*-aminophenol (PAP) in the presence of $NaBH_4$. The generated PAP was electrooxidized to *p*-quinone imine (PQI) with

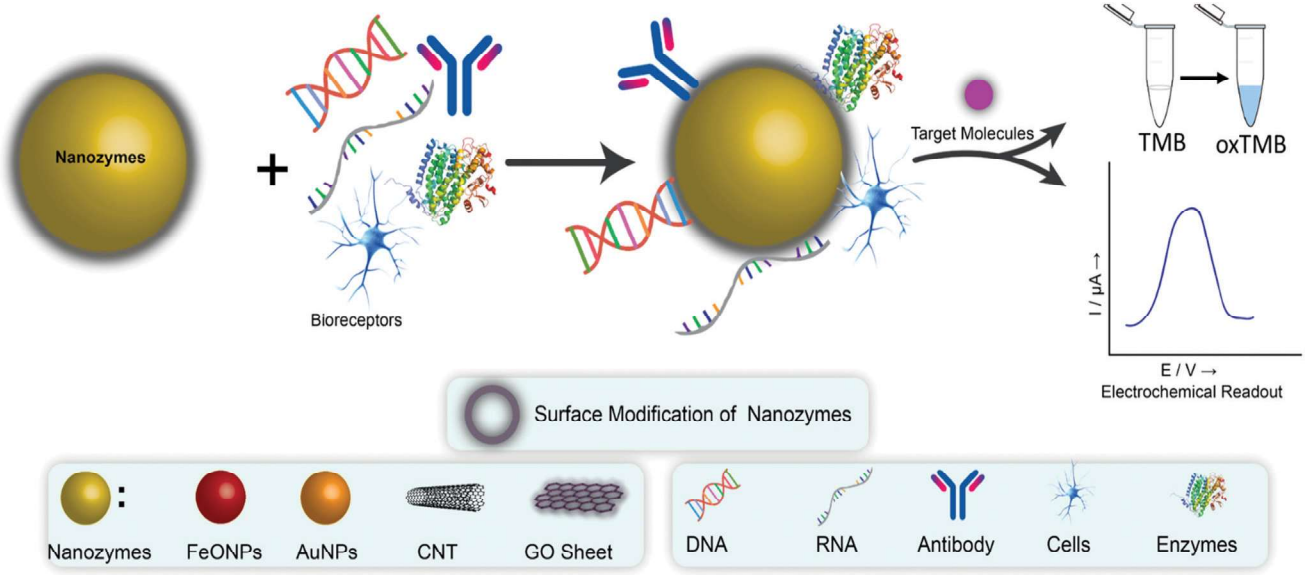

Fig. 4 Schematic representation of the nanozyme's catalytic activities and its application in the electrochemical biosensor. Nanozymes can be functionalized with a range of receptor probes (*e.g.*, complementary capture probes for DNA and RNA targets, antibodies for proteins, *etc.*) by conventional surface modification procedures. The probe-functionalized nanozymes can capture the targets (*e.g.*, pathogens, cancer cells, exosomes, nucleic acids) *via* the specific interaction between nanozyme-bound probes and targets. The nanozyme-attached targets can then be quantified electrochemically or optically (*i.e.*, naked eye and UV-visible) *via* an ELISA-type sandwich immunoassay or sandwich hybridization method.

ferrocenecarboxylic acid (FCA) in the solution. The produced PQI was then reduced back to PAP by $NaBH_4$, leading to the redox cycling between PAP and PQI. As a result, an enhanced electrochemical response was produced which allows one to achieve a high sensitivity with 3-orders of magnitude higher than that of AuNP labels alone. This sensor was able to detect as low as 0.3 aM DNA. In another strategy, Ling *et al.* reported an electrochemical DNA quantification method based on the nanozyme activity of the MOF nanostructure and the allosteric switch of hairpin DNA (Fig. 5).[69] Initially, a glassy carbon electrode was functionalized with the streptavidin (SA) aptamer sequence of a hairpin DNA. Due to its loop structure, electrode-bound hairpin DNA is inaccessible to SA attached conjugates. Upon the addition of target DNA, the loop bound to the target sequence and unfolded the stem of hairpin DNA, making it accessible for SA attached conjugates to form a structure with the combinative SA aptamer. The surface-bound activated DNA selectively bound with the SA coated FeTCPP@MOF *via* a specific interaction between the SA-apatamer and SA. The nanozyme activity of FeTCPP@MOF was then used to catalyse the oxidation of *o*-phenylenediamine (*o*-PD) in the presence of H_2O_2. This assay demonstrates a good performance for the detection of DNA with a LOD down to 0.48 fM, a 6-order magnitude linear range, a single mismatch differentiation ability, and practical application in complex samples. This study opens up a new direction of functionalized MOFs as nanozymes for signal transduction in electrochemical biosensing and shows better enzymatic activities due to their natural enzyme-like metal center and porous nanostructure.

MicroRNAs (miRNAs) are small (~17–25 nucleotides long), single-stranded noncoding RNA molecules that suppress the expression of protein-coding genes by translational repression, messenger RNA degradation, or both and are involved in early events in disease progression.[172,173] In recent years, circulating miRNAs and exosomal miRNAs (*exo*-miRNA) have been used as diagnostic and prognostic markers for a range of diseases, including cancer.[174–177] Quantitative real-time PCR (q-PCR), reverse transcription polymerase chain reaction (qRT-PCR), *in situ* hybridization, northern blotting, RNA-seq analysis, microarray, and next-generation sequencing are some of the techniques that have been widely used for the quantification of RNA markers in bodily fluids. These techniques are particularly suitable for biomarker discovery, and none of these techniques serves the purpose of on-site or POC detection.[178] In contrast, the nanozyme based electrochemical miRNA sensor provides rapid analysis along with adequate sensitivity. Li *et al.* developed a miRNA sensor to detect miRNA-122,[67] a biomarker

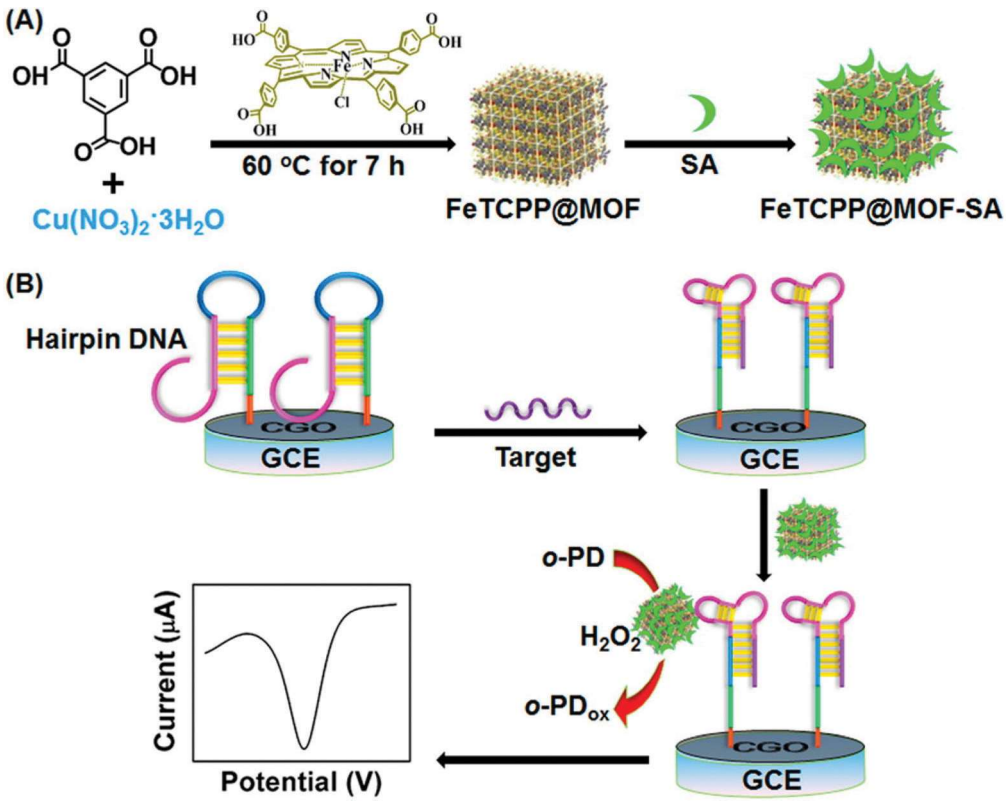

Fig. 5 (A) Synthesis of FeTCPP@MOF nanozymes followed by covalent coupling with streptavidin (SA) to form the FeTCPP@MOF-SA composite and (B) target binding initiates the allosteric switch of the hairpin probe allows FeTCPP@MOF-SA to recognize the probe and *o*-PD oxidation provides the electrochemical signal. Reprinted with permission from ref. 69 (DOI:10.1021/acs.analchem.5b00001). Copyright (2015) American Chemical Society.

of drug-induced liver injury. The nanozyme activity of palladium nanoparticle based MOF nanohybrids was used. The nanohybrid enzymes were utilized both as nanocarriers to immobilize a large amount of biotin-labeled signal probes (H2) and as tracers to quickly catalyze the oxidation of TMB in the presence of H_2O_2. The target miR-122 was sandwiched between the tracers and electrode-bound thiolated capture probes (H1). With the help of the target-catalyzed hairpin assembly (TCHA), target miR-122 triggered the hybridization of H1 and H2 for further release to initiate the next reaction process resulting in numerous tracers anchored onto the sensing interfaces. Due to dual signal amplification (*e.g.*, target induced signal amplification and TMB oxidation by the tracer indicator PdNPs@Fe-MOF), this method could detect miRNA-122 as low as 0.003 fM in human serum.[67]

6.2 Cytosensor

Circulating tumor cells (CTCs) have emerged as a valuable tool that can provide mechanistic insights into the tumor heterogeneity, clonal evolution, and stochastic events within the metastatic cascade. They are regarded as one of the most promising biomarkers for early diagnosis of cancer.[179] As a general strategy of CTC detection, antibody- or aptamer-anchored (for aptasensors see section 6.4) nanoprobes are designed to target abnormal and/or overexpressed cell surface receptors (proteins) or other cell surface components, including glycans, folic acid, and sialic acid.[170,179] However, the low abundance (1–10 CTCs for 1 billion of blood cells)[179] and inherent fragility of CTCs pose great challenges for CTC detection. To enhance the sensitivity of CTC analysis, Tian *et al.* have developed an ultrasensitive electrochemical sensor using a reduced graphene oxide/molybdenum disulfide (rGO/MoS_2) composite modified magnetic glassy carbon electrode (MGCE) as a detector, and aptamer modified magnetic Fe_3O_4NPs as dispersible capture agents.[82] Cancer cells were attached with the aptamer modified Fe_3O_4NPs *via* the aptamer–antigen interaction. The cell-attached conjugates were then magnetically attached onto the rGO/MoS_2 composite-modified electrode. An enhanced electrochemical signal was achieved due to the nanozyme catalytic oxidation of TMB on rGO/MoS_2 composites with the Fe_3O_4NP binanozyme surface. The method was able to detect 6 MCF-7 cells per mL which showed significant improvement from their previous report with the rGO/AuNP modified GCE and the MUC-1 aptamer modified CuO nanozyme (LOD 27 cells per mL).[58] Very recently, Alizadeh *et al.* proposed a "signal-off" strategy to detect cancer cells. CuO/WO_3 nanoparticle decorated graphene oxide nanosheets (CuO/WO_3-GO) were modified with folic acid (FA), and were then absorbed on cancer cells *via* a folic acid targeting ligand. In this strategy, the peroxidase like-activity of CuO/WO_3-GO was used to oxidise *o*-phenylenediamine in the presence of H_2O_2. During the interaction between cells and CuO/WO3-GO, some amount of H_2O_2–OPD system participated in a chemical reaction and removed from the electrode, resulting in a decrease in the response signal. Using this principle, the authors successfully achieved a detection limit of 18 cells per mL.[29]

6.3 Immunosensor

The basis of electrochemical immunosensors is the non-covalent interaction between an antigen and antibody to form a sandwich-type architecture on the electrode surface. In a conventional system, an enzyme-labelled antibody or antigen amplifies the immune-capture event that can be quantified by voltammetric or amperometric readout methods.[170,180] In this regard, successful conjugation of the antibody or antigen with an enzyme is crucial. However, most of the standard conjugation, separation and purification methods for enzyme-conjugated antibodies or antigens suffer from expensive, time consuming, multistep and laborious procedures. For example, during the conjugation of the antibody with the nanozyme, nearly all nanozyme labelled antibodies settle down through centrifugation at a relatively lower RPM, which adds an extra degree of complexity to the immunosensor fabrication process. Nanozyme–antibody conjugation can be achieved *via* either electrostatic interactions between them or chemical reactions between the carboxylic acid (–COOH) or amine ($–NH_2$) groups of functionalized nanozymes with the $–NH_2$ acid –COOH groups of the antibody. For instance, it was reported that the $–NH_2$ groups of secondary antibodies (Ab_2) electrostatically interacted with Au@Pt (Au–N and Pt–N) of Co_3O_4@CeO_2-Au@Pt nanozymes and were used as labels in a sandwich-type electrochemical immunosensor to detect the squamous cell carcinoma antigen. This sensor showcased an excellent sensitivity due to the surface area for Ab_2 immobilization and the synergic effect of the Co_3O_4@CeO_2-Au@Pt nanozyme towards H_2O_2 reduction. This assay offered a LOD of 33 fg mL^{-1}.[181] Wei *et al.* also published a similar approach for the quantitative detection of the hepatitis B surface antigen using MoS_2@Cu_2O-Pt nanozymes.[182]

Although nanozyme-based sensors are well known for amplifying the readout signals (*i.e.*, "signal-on"), they can equally be useful in generating a noticeable change in electrochemical response in "signal-off" sandwich immunosensing strategies. This method generally involves a nanozyme catalyzed chemical reaction that forms a nonconducting precipitate on the electrode surface. The precipitate blocks the working area of the electrode and thus hinders the electron transfer reaction between the solution-phase electroactive species and the electrode. In some cases, the precipitate may reduce the concentration of the electroactive species (see section 6.2). For instance, Zhang *et al.* developed a "signal-off" sandwich immunosensor to detect α-fetoprotein. After the successful immune-recognition of FeS_2-AuNPs-Ab_2 on the electrode surface, FeS_2-AuNP nanozymes catalyze 4-chloro-1-naphthol in the presence of H_2O_2 to form insoluble precipitation. Thus, a reduced differential pulse voltammetric response of electroactive nickel hexacyanoferrate nanoparticles (NiHCFNPs) was observed.[183]

Recently Shiddiky's group has developed an immunosensor to detect the p53 autoantibody in serum and highlighted that the method could be adopted for virtually any type of protein biomarker.[54] In this method, the surface of a new class of

nanozymes, gold-loaded nanoporous Fe_2O_3 nanocubes (Au–$NPFe_2O_3NC$), was modified with IgG and was used as labels in the sandwich immunodetection of autoantibodies. As shown in Fig. 6, a biotinylated p53 antigen was attached to a neutravidin-modified screen-printed carbon electrode *via* the biotin–neutravidin affinity interaction. This electrode was then incubated with the serum sample to capture the target p53 autoantibody present within the sample. The IgG/Au–$NPFe_2O_3NC$ is used to recognize electrode-bound autoantibodies. The nanozyme activity of IgG/Au–$NPFe_2O_3NC$ was to adopt an ELISA-based sensing protocol where the oxidation of TMB in the presence of hydrogen peroxide was mimicked to generate coloured complexes for naked-eye observation and electrochemical detection of target autoantibodies. The electrochemical quantification has been carried out using a new screen-printed electrode. The most attractive feature of this sensor is that the high surface area and enhanced nanozyme activity of the Au–$NPFe_2O_3NC$ offer enhanced sensitivity (*i.e.*, LOD of 0.08 U mL^{-1}) in the immunodetection of autoantibodies in biological fluids. Although this sensitivity is enough to detect the p53 autoantibody in the clinical sample, it cannot obsolete the HRP based sensor having a LOD of 0.02 U mL^{-1}, previously reported by the same group.[54,73]

The nanozyme activity of Au–$NPFe_2O_3NC$s has been used to develop a simple method for direct isolation and subsequent detection of a specific population of exosomes.[55] In this method, the Au–$NPFe_2O_3NC$s were initially functionalized with a generic exosome-associated antibody (*i.e.*, CD63) and dispersed in the target samples where they work as "dispersible nanocarriers" to capture the bulk population of exosomes. After magnetic collection and purification, Au–$NPFe_2O_3NC$-bound exosomes were transferred to the disease-specific antibody-modified electrode. As a proof of principle, they used a specific placental marker, placenta alkaline phosphatase (PLAP), to detect exosomes secreted from placental cells. The nanozyme activity of Au–$NPFe_2O_3NC$ was then used to accomplish a naked-eye observation along with UV–visible and electrochemical detection of PLAP-specific exosomes present in placental cell-conditioned media. They showed an excellent agreement in analytical performance for their methods using with and without the commercial "total exosome isolation kit"-based pre-isolation step.

Shiddiky's group also developed another class of mesoporous iron oxide materials and demonstrated their nanozyme activity in the immune detection of DNA methylation.[53] In this method, the target DNA was first extracted and denatured to get ssDNA followed by direct adsorption onto the surface of a bare screen-printed gold electrode. 5-Methylcytosine antibody (5mC) functionalized mesoporous iron oxide materials were then used to recognize the methyl cytosine groups present on the electrode. The nanozyme–5mC conjugates catalyse the TMB solution to give the naked-eye observation and electro-

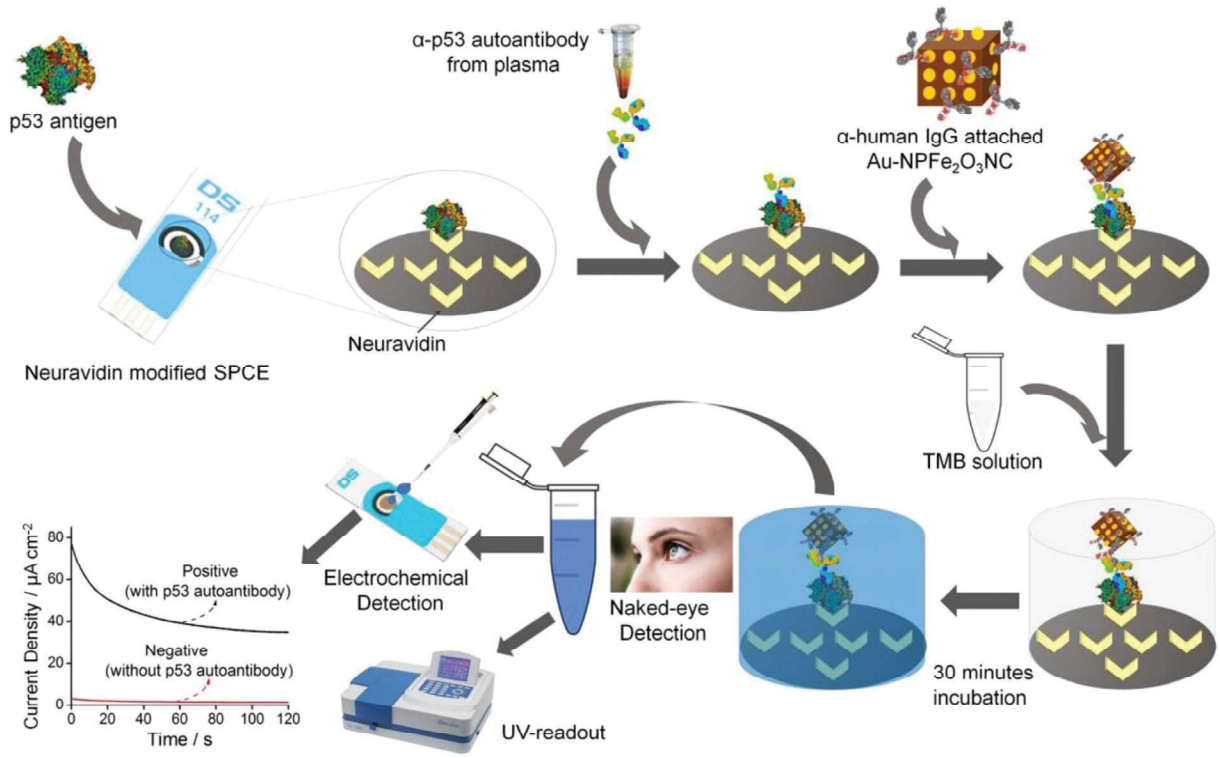

Fig. 6 Schematic representation of naked eye and electrochemical detection of the p53 autoantibody where target recognition and electrochemical measurement are operated in two separated electrodes. Reprinted with permission from ref. 54 (DOI:10.1021/acs.analchem.5b00001). Copyright (2017) American Chemical Society.

chemical detection of DNA methylation. The assay successfully detected as low as 10% difference in the global DNA methylation level in synthetic samples and cell lines with good reproducibility and specificity. This strategy avoids the use of HRP, traditional PCR based amplification and bisulfite treatment steps that are generally used in many conventional DNA methylation assays.

6.4 Aptasensor

Aptamers are ssDNA or RNA molecules synthesized by SELEX (systematized exponentially enriched ligands) with a unique two- or three-dimensional structure that binds to a specific target molecule.[184] Due to their strong affinity (*i.e.*, high specificity to the target), small size, excellent stability, and flexibility in modification, aptamers become a strong competitor of antibodies.[21,50,185] In recent years, nanozyme conjugated aptamers have been used for detecting whole cells,[58] pathogens,[50] and proteins.[75,76,79] Sun *et al.* developed a method to detect cardiac troponin I (cTnI), a gold standard marker for acute myocardial infarction (AML) found in the bloodstream, where nanozymes were used for catalytic signal enhancement. This sensor was fabricated by immobilizing nanotetrahedron (NTH) based dual aptamers (Tro4 and Tro6) on the screen-printed gold electrode.[75] After binding of target (cTnI) aptamer modified Fe_3O_4@UiO-66/Cu@Au (nanoprobe-1), it was dispensed on the electrode surface to form a super-sandwich-like structure. Nanoprobe-1 could oxidize HQ in the presence of H_2O_2 through multiple nanozyme activities attributed to Fe_3O_4@UiO-66 and Cu@Au (Fig. 7). Additionally, attachment of super-sandwich and cDNA (complementary to aptamers) modified Cu@Au through hybridization forms a cluster-based nanoprobe, which could further increase the catalytically active sites for the HQ/H_2O_2 system, resulting in a more sensitive catalytic response.[75] A more sensitive electrochemical assay for the detection of cTnI was fabricated using co-catalysis of magnetic Fe_3O_4 nanocarriers loaded with natural HRP, Au@Pt nanozyme and G-quadruplex/hemin DNAzyme (7.5 *vs.* 16 pg mL^{-1}).[74] In both the cases, NTH helps to maintain precise orientation of aptamers on the sensing surfaces, providing a native-like microenvironment for cTnI binding.

Recently, gold nanozyme based aptasensors have been developed for detection of pathogens.[21] In 2019, Bansal's group developed an electrochemical sensor for the detection of the *Pseudomonas aeruginosa* (PA) bacterial pathogen using the nanozyme activity of AuNPs and the high affinity and specificity of a PA-specific aptamer (F23).[50] The presence of an aptamer inhibits the inherent peroxidase-like activity of GNPs by simple adsorption onto the surface of GNPs. In the presence of target pathogens, the aptamer leaves the AuNP surface, allowing them to resume their peroxidase-like activity, resulting in the oxidation of TMB at the screen-printed carbon electrode. The method is sensitive to detect PA with a LOD of ~60 CFU mL^{-1} in water within 10 min. The authors envisaged

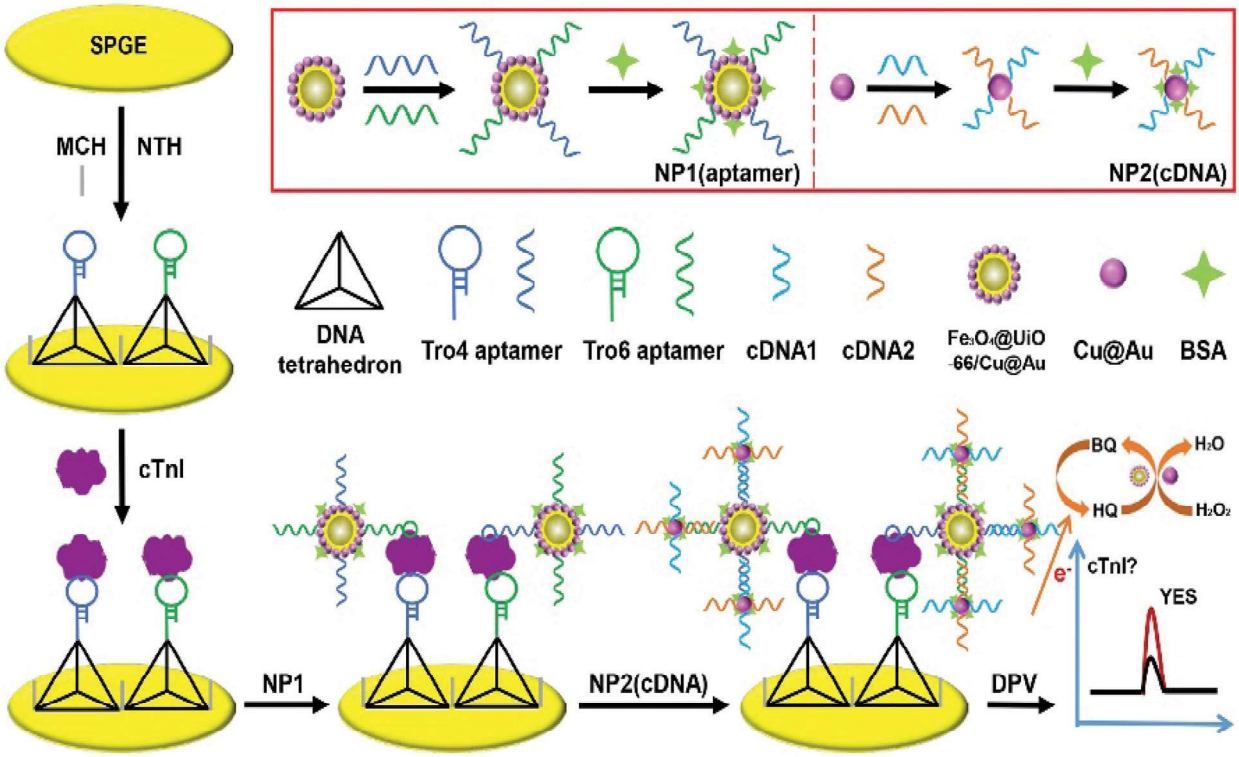

Fig. 7 Schematic representation of the layer-by-layer (LBL) assembly of the nonenzymatic nanoprobes NP1 (aptamer) and NP2 (cDNA) and the NTH-assisted dual-aptamer based electrochemical sensor for detection of cTnI. Reprinted from ref. 75 (DOI:10.1016/j.bios.2019.03.049), Scheme 1, Copyright (2019), with permission from Elsevier.

that this assay might become a generic platform to detect other molecular and cellular analytes.

6.5 Small molecule detection

Small molecules include heavy metal ions and low molecular weight organic compounds such as drugs, toxins (*e.g.*, ochratoxin A), pesticides, antibiotics (*e.g.*, kanamycin A), amino acids (*e.g.*, biothiols: cysteine, glutathione), intermediate of sugars (*e.g.*, glucose), lipids (*e.g.*, cholesterol), second messengers (*e.g.*, cAMP, cGMP), metabolites of cellular respiration (*e.g.*, lactate) *etc*.[186–189] Some of these molecules are essential biomarkers for many diseases. Thus, measuring the concentration of a given small molecule in bodily fluids (*i.e.* whole blood, serum, urine, saliva, tear, and sweat) is an effective way to diagnose a disease. For example, the blood glucose level is an indicator of diabetes: hyperglycemia and hypoglycemia,[190,191] and the blood lactate level can predict multiple system organ failure (MSOF) caused by septic shock[192] and ischemia and inadequate oxygenation.[193] Over the years, a number of enzyme-mimicking nanostructured materials[188,193–204] have been used for the detection of glucose,[194–197,202,203] lactate,[193,198,199,204] uric acids,[200] kanamycin,[188] and arsenate.[201] In this section, nanozyme based electrochemical sensors for glucose detection are briefly discussed.

The majority of electrochemical glucose sensors worked based on the direct enzymatic oxidation of H_2O_2 at the GOx-modified electrode. This design commonly suffers from the interference of ascorbic acid (AA), uric acid (UA), 4-acetaminophen (AP) and other electroactive species present in the blood. This problem can be avoided by using the enzymatic reduction of H_2O_2 at relatively low potential. Gao *et al.* developed a glucose sensor based on the co-immobilizing of Prussian blue (PB) and GOx on TiO_2 nanotube arrays (TiNTs).[203] In this assay, PB reduced H_2O_2 at relatively low potential. The sensor demonstrated not only high selectivity to glucose, but also a fast response (1 s) and broad dynamic range (0.01 to 0.70 mM) with a detection limit of 3.2 mM. Recently, Shiddiky's group reported a dual-mode (colorimetric and electrochemical) glucose sensor, where the peroxidase-mimicking activity of mesoporous Fe_2O_3 nanozymes was used to catalyse the oxidation of TMB in the presence of *in situ* enzymatically produced H_2O_2. Both the colorimetric (naked-eye and UV–vis) and electrochemical assays estimated the glucose concentration to be in the linear range from 1.0 μM to 100 μM with a detection limit of 1.0 μM.[194]

7. Applications of nanozymes in microfluidic assays

Microfluidics is a science and technology of handling and precise controlling of the sub-milliliter volume of fluids in micrometre-scale platforms.[205,206] There are several formats of microfluidics, including continuous-flow microfluidics, paper-based microfluidics (also known as microfluidic paper-based analytical devices (μPADs)), digital and droplet-based microfluidics.[207,208] The synergistic combination of these formats of microfluidics with biosensors can increase the sensitivity, selectivity and portability, while decreasing the LOD and overall footprint of such analytical devices.[209,210] Moreover, integrated, microfluidic biosensors can realise the real-time and multianalyte detection of various biomarkers.

Nanozymes have also been used in such microfluidic biosensors that function mainly based on colorometric, fluorescent and electrochemical detection methods. One of the early works in this field was based on a versatile microfluidic device, termed a multiplexed volumetric bar-chart chip (V-Chip).[211] The V-Chip efficiently measured the oxygen gas produced as a result of decomposition of hydrogen peroxide in the presence of PtNPs.[212] Combined with the ELISA technique, it was shown that the V-Chip could efficiently detect cancer biomarkers both in serum and on the cell surface. Later, this microfluidic chip was integrated with a target-responsive hydrogel containing Au@PtNPs for quantitative POC testings.[213]

Nanozyme-based colorometric μPADs are also accessible, cost-effective and relatively simple analytical platforms that have an excellent commercialization capability in this field. Such analytical devices can be integrated with off-the-shelf equipment such as smartphones for further processing the analytical signals. For instance, Han *et al.* incorporated AuNPs in a μPAD to colorimetrically detect mercury ions (Hg^{2+}) in water samples. The intensity of the colorimetric detection correlated well with the efficient reaction of Au–Hg facilitated by gold NPs in the fabricated μPAD. Using a MOF as a peroxidase mimic to oxidase TMB in the presence of H_2O_2, a colorimetric μPAD-based biosensor was also developed for glucose monitoring.[214] The μPAD could also be integrated with a smartphone for quantitative analysis of the generated color. Zhang *et al.* used modified carbon nitride nanozymes for colorimetric detection of glucose.[215] Using a microfluidic device for real-time monitoring, their developed microfluidic platform with metal-free nanozymes could detect glucose with a LOD as low as 0.8 μM within 30 seconds.

Through incorporating zeolitic imidazolate framework (ZIF-8) based nanozymes in an I-shaped microfluidic channel and using a fluorescence detection technique, Cheng *et al.* realized an *in vivo*, real-time, continuous biosensor platform.[216] To sensitively detect the secreted hydrogen peroxide from single cells, a droplet-based microfluidic platform has also been developed in the literature.[217] A high fluorescence signal generated with the hybridization of HRP with gold nanoclusters trapped in a 4.2 nL droplet led to the sensitive detection of H_2O_2.

A rapid and efficient microfluidic-based nanozyme-mediated electrochemical detection device for targeted genetic analysis was developed by Koo *et al.*[218] The authors fabricated an electrode-patterned microfluidic chip with one central lysis chamber and four amplification chambers. The surface of the amplification chambers was immobilized with superparamagnetic iron oxide NPs to detect circulating tumor nucleic

acids (ctNA) in the urine and blood of patients with prostate cancer. An electrochemical-based microfluidic POC device for real-time detection of H_2O_2 was also fabricated.[219] It was shown that a stable biosensor with tremendous peroxidase-like catalytic activity and a LOD as low as 1.62 μM can be realized by immobilization of gold and platinum NPs with GO inside a hydrogel microbead.

8. Challenges in nanozyme-based electrochemical biosensors and potential solutions

Although nanozyme-based electrochemical biosensors are promising platforms for detecting various analytes of interest quickly and reliably, they suffer from the combined technical and clinical challenges associated with both nanozymes and electrochemical biosensors.

8.1 Technical challenges associated with nanozymes

8.1.1 Limited enzyme-mimicking activities of nanozymes. One of the major issues of nanozymes that need continuous improvement is their enzyme-mimicking activities. To this aim, synthesizing more robust nanozymes that better exhibit the properties of natural enzymes are in demand. In particular, the current advances in nanotechnology, artificial intelligence and computational chemistry can significantly improve the oxidoreductase activity of nanozymes for electrochemical detection.

8.1.2 Low specificity of nanozymes. The inherently low specificity of nanozymes is another limitation of nanozymes. Unlike natural enzymes, nanozymes lack precise binding sites to interact with a substrate appropriately. This issue of lacking the substrate-binding sites significantly affects the specificity of nanozymes; thus, modification/engineering of the nanozymes is required to improve their specificity. Moreover, high specificity is critically important in biomolecular sensing for various biomedical applications, especially for disease diagnosis and monitoring. As such, nanozymes with highly improved specificity need to be used in electrochemical biosensors for disease detection.

8.1.3 Low catalytic activities of nanozymes. Another inherent problem of nanozymes is their relatively low catalytic activities compared to those of natural enzymes. The relatively low catalytic activities of nanozymes significantly compromise their bioconjugation. This limitation can be addressed by using molecularly imprinted polymers (MIPs) on nanozymes[220] as well as synthesizing the so-called integrated nanozymes.[38] MIPs improve the specificity and catalytic activity through generating binding sites on the substrate by polymerization. In INAzymes, the natural enzymes are combined with nanozymes in a 3D network structure to improve the selectivity and catalytic activity. Among various 3D network structures required to fabricate such a hybrid enzyme-mimicking nanomaterial, MOFs hold great promise.[221] Using MIP- or MOF-based hybrid nanozymes in electrochemical biosensors can significantly improve the selectivity of the system.

8.1.4 Poor reproducibility of nanozymes. The poor reproducibility of nanozymes is a significant problem that potentially hinders the widespread application of nanozyme-based electrochemical biosensors. This issue mainly arises for two reasons. Firstly, small-scale synthesis in the individual lab does not guarantee the size, shape, and porosity of nanoparticle from different batches, leading to activity changes. Secondly, bioconjugation between the recognition element and nanozyme is highly subjective and depends on an individual's expertise and considerations. Therefore, essential efforts need to be taken for the industrial production and standardization of effective bioconjugation protocols.

8.2 Clinical challenges associated with nanozyme-based electrochemical biosensors

8.2.1 False-positive results in clinical samples. The conductivity and catalytic activity of nanozymes can significantly improve the sensitivity of electrochemical biosensors. Nevertheless, clinical samples, such as patients' blood and urine, contain complex biological matrices, including thousands of unwanted proteins, cells, lipids and nucleic acids. These complex biological matrices can be adsorbed nonspecifically on the surface of the electrochemical sensors and eventually lead to a false-positive result. As such, the surface of the electrochemical sensor needs to be coated with nonspecific binding agents such as bovine serum albumin (BSA) and polyethylene glycol (PEG). Moreover, the aggregation of nanozymes can also interfere with the signal transduction, thus reducing the specificity of the biosensor. To address this issue, it is recommended that the solution containing nanozymes be kept away from UV sources and reactive oxygen species (ROS)-rich environments. Finally, a specific recognition probe such as an aptamer-nanozyme probe can be implemented into the detection device to improve the specificity of the device.

8.2.2 Biofouling. Biofouling of the electrode surface is a significant clinical challenge that can hinder nanozyme-based electrochemical biosensors for clinical applications. The problem of biofouling of the electrodes is more highlighted when electrochemical biosensors are being used for detecting disease-specific biomarkers in bodily fluids. Since the electrodes are in direct contact with bodily fluids such as blood, urine, plasma, or serum, unwanted cells, proteins, and other biomolecules may attach to the electrode surfaces *via* a nonspecific interaction. This can adversely affect the specificity and decrease the signal-to-noise ratio. To address this problem, the surface of the electrode needs to be coated with anti-fouling materials such as zwitterionic polymers, peptides, and polyethene glycol.[222]

8.2.3 Lack of standard protocols for synthesis and bioconjugation. Although nanozymes are highly versatile, stable, and inexpensive, their synthesizing methods may differ from one lab to another. Also, the fabrication techniques of nanozymes are highly subjective, and the bioconjugation process may depend on individuals' skills. As such, nanozyme-based

electrochemical biosensors may suffer from poor reproducibility, which is a crucial factor affecting their acceptance for real clinical settings. Therefore, this field can significantly benefit from standardization and automation. In this regard, the integration of these systems with the microfluidic technology can be highly beneficial and has the potential to address these limitations. For instance, the synthesizing methods of nanozymes and the bioconjugation process involve many steps of mixing, washing, and separation. These steps are usually performed using rotating lab shakers and centrifuge machines whose durations mainly differ from one lab to another. On the other hand, mixing and separation in microfluidic devices are highly efficient and can be efficiently streamlined.[223]

8.2.4 Lack of an automated nanozyme-based electrochemical biosensing platform for point-of-care testing. To address the issue of automation of nanozyme-based electrochemical biosensors for POC testing and disease detection, it would be highly required to integrate the whole process of isolation, separation, and detection of the pathogenic targets on the same device. This concept is closely related to lab-on-a-chip or micro total analysis systems that are currently being practised for many chronic diseases such as cancer[224] and autoimmune disorders.[225]

9. Concluding remarks and future perspectives

The last decade witnessed an overwhelming surge in research about nanozymes and expansion of their applications to biomedical sensing, therapeutics, and environmental engineering. Herein, we summarize the representative enzyme mimics and plausible catalytic mechanism, and a particular focus has been given to the recent updates in nanozyme based electrochemical detection of clinically relevant biomarkers (*e.g.*, DNA, miRNA, protein, and CTCs). Dynamic progress in this field endows nanozymes with enormous functionalities such as nanocarriers, robust catalytic behaviour, probe immobilizers, conductive surface modifiers and signal generators or tracer tags. Until now, few nanozymes have shown catalytic activity as natural counterparts, but the majority manifest moderate to low activity. Although heteroatom doping, composite or bimetal formation may increase the activity significantly, the improvement in substrate selectivity remains low. On the other hand, molecular imprinting or surface modifications improve molecular recognition and substrate selectivity sacrificing activity. In this direction, a better understanding of structure–activity relationships, the rational design of nanomaterials, experimental and computational studies are pivotal to elucidate the catalytic mechanism and impart maximum activity and selectivity at the same time or balancing them for a particular application.

One of the critical issues is the multi-enzymatic property, which has been proved to be useful in therapeutic purposes. Still, how this could be beneficial to design and fabricate solid-state immunoassays (ELISA, LFIA) and electrochemical sensors is not properly addressed. Moreover, over the years, most of the sensors have utilized HRP-mimicking nanomaterials. Thus, the majority of nanozymes have remained unexplored. The development of multifunctional nanozymes could be a challenging and interesting topic for the coming days. Besides catalysis, specific physicochemical properties such as magnetic, optical, or thermal properties would capacitate enzyme mimics to be realized for ultra-sensitive and user-friendly detection of a biomolecule from complex body fluids.

Finally, the combination of this field with microfluidics can streamline many tedious and highly-subjective processes of synthesis and bioconjugation. For instance, replacing the laboratory shakers and centrifuge machines with efficient micromixers and microfluidic-based particle separation devices can facilitate the automation and standardization of this field. Moreover, integrating the whole process of isolation separation and detection of the pathogenic targets on a single chip can revolutionize the applications of nanozyme-based electrochemical biosensors for disease diagnosis and monitoring of the therapy effectiveness.

Abbreviations

ABTS	2,2′-Azino-bis-3(ethylbenzthiazoline-6-sulfonic acid)
Au@PtNPs	Gold core/platinum shell nanoparticles
BPDE	Benzo[*a*]pyrene-7,8-diol 9,10-epoxide
CHA	Catalytic hairpin assembly
ctDNA	Circulating tumor deoxyribonucleic acid
CNTs	Carbon nanotubes
DAB	3,3′-Diaminobenzidine
DNC	Dextran-coated nanoceria
dsDNA	Double-stranded deoxyribonucleic acid
EBOV	Ebolavirus
ELISA	Enzyme-linked immunosorbent assay
FCA	Ferrocene carboxylic acid
GO	Graphene oxide
GOx	Glucose oxidase
GPx	Glutathione peroxidase
HRP	Horseradish peroxidase
IONPs	Iron oxide nanoparticles
IONzyme	Iron oxide nanozyme
LFBs	Lateral flow biosensors
LFIAs	Lateral flow immunochromatographic assays
MNP	Magnetic nanoparticle
MOFs	Metal–organic frameworks
NPs	Nanoparticles
OPD	*o*-Phenylenediamine dihydrochloride
PAP	*p*-Aminophenol
PB	Prusian blue
PQI	*p*-Quinone imine
PNP	*p*-Nitrophenol
PtNCs	Platinum nanocatalysts
POC	Point-of-care
rGO	Reduced graphene oxide

SOD	Superoxide dismutase
ssDNA	Single-stranded deoxyribonucleic acid
TEP	Triethylphosphite
TMB	3,3′,5,5′-Tetramethylbenzidin
TTMPP	Tris(2,4,6-trimethoxyphenyl)phosphine

Conflicts of interest

Q6 ■■■■

Acknowledgements

This work was partly supported by the Australian Research Council (ARC) Discovery Projects (DP180100055, DP190102944) and the National Research Foundation of Korea (NRF) grant (2019R1A2C1002531) funded by the Korean government.

References

1 F. Manea, F. B. Houillon, L. Pasquato and P. Scrimin, *Angew. Chem., Int. Ed.*, 2004, **43**, 6165–6169.
2 J. Wu, X. Wang, Q. Wang, Z. Lou, S. Li, Y. Zhu, L. Qin and H. Wei, *Chem. Soc. Rev.*, 2019, **48**, 1004–1076.
3 L. Gao, J. Zhuang, L. Nie, J. Zhang, Y. Zhang, N. Gu, T. Wang, J. Feng, D. Yang, S. Perrett and X. Yan, *Nat. Nanotechnol.*, 2007, **2**, 577–583.
4 Y. Huang, J. Ren and X. Qu, *Chem. Rev.*, 2019, **119**, 4357–4412.
5 D. Jiang, D. Ni, Z. T. Rosenkrans, P. Huang, X. Yan and W. Cai, *Chem. Soc. Rev.*, 2019, **48**, 3683–3704.
6 J. Wu, S. Li and H. Wei, *Nanoscale Horiz.*, 2018, **3**, 367–382.
7 X. Zheng, Q. Liu, C. Jing, Y. Li, D. Li, W. Luo, Y. Wen, Y. He, Q. Huang, Y. T. Long and C. Fan, *Angew. Chem., Int. Ed.*, 2011, **50**, 11994–11998.
8 W. Luo, C. Zhu, S. Su, D. Li, Y. He, Q. Huang and C. Fan, *ACS Nano*, 2010, **4**, 7451–7458.
9 X. Shen, W. Liu, X. Gao, Z. Lu, X. Wu and X. Gao, *J. Am. Chem. Soc.*, 2015, **137**, 15882–15891.
10 L. Jin, Z. Meng, Y. Zhang, S. Cai, Z. Zhang, C. Li, L. Shang and Y. Shen, *ACS Appl. Mater. Interfaces*, 2017, **9**, 10027–10033.
11 Z. Gao, M. Xu, L. Hou, G. Chen and D. Tang, *Anal. Chim. Acta*, 2013, **776**, 79–86.
12 R. Polsky, R. Gill, L. Kaganovsky and I. Willner, *Anal. Chem.*, 2006, **78**, 2268–2271.
13 T. Li, Y. Du and E. Wang, *Chem. – Asian J.*, 2008, **3**, 1942–1948.
14 J. Lan, W. Xu, Q. Wan, X. Zhang, J. Lin, J. Chen and J. Chen, *Anal. Chim. Acta*, 2014, **825**, 63–68.
15 Q. Wang, X. Zhang, L. Huang, Z. Zhang and S. Dong, *Angew. Chem., Int. Ed.*, 2017, **56**, 16082–16085.
16 Y. Hu, H. Cheng, X. Zhao, J. Wu, F. Muhammad, S. Lin, J. He, L. Zhou, C. Zhang, Y. Deng, P. Wang, Z. Zhou, S. Nie and H. Wei, *ACS Nano*, 2017, **11**, 5558–5566.
17 L. Gao, K. Fan and X. Yan, *Theranostics*, 2017, **7**, 3207–3227.
18 H. Cheng, L. Zhang, J. He, W. Guo, Z. Zhou, X. Zhang, S. Nie and H. Wei, *Anal. Chem.*, 2016, **88**, 5489–5497.
19 P. Weerathunge, R. Ramanathan, R. Shukla, T. K. Sharma and V. Bansal, *Anal. Chem.*, 2014, **86**, 11937–11941.
20 R. S. Li, H. Liu, B. Bin Chen, H. Z. Zhang, C. Z. Huang and J. Wang, *Anal. Methods*, 2016, **8**, 2494–2501.
21 P. Weerathunge, R. Ramanathan, V. A. Torok, K. Hodgson, Y. Xu, R. Goodacre, B. K. Behera and V. Bansal, *Anal. Chem.*, 2019, **91**, 3270–3276.
22 T. K. Sharma, R. Ramanathan, P. Weerathunge, M. Mohammadtaheri, H. K. Daima, R. Shukla and V. Bansal, *Chem. Commun.*, 2014, **50**, 15856–15859.
23 H. Cheng, S. Lin, F. Muhammad, Y.-W. Lin and H. Wei, *ACS Sens.*, 2016, **1**, 1336–1343.
24 X. Wang, L. Qin, M. Zhou, Z. Lou and H. Wei, *Anal. Chem.*, 2018, **90**, 11696–11702.
25 Z. Zhu, Z. Guan, S. Jia, Z. Lei, S. Lin, H. Zhang, Y. Ma, Z.-Q. Tian and C. J. Yang, *Angew. Chem., Int. Ed.*, 2014, **53**, 12503–12507.
26 D. Duan, K. Fan, D. Zhang, S. Tan, M. Liang, Y. Liu, J. Zhang, P. Zhang, W. Liu, X. Qiu, G. P. Kobinger, G. F. Gao and X. Yan, *Biosens. Bioelectron.*, 2015, **74**, 134–141.
27 J. Han, L. Zhang, L. Hu, K. Xing, X. Lu, Y. Huang, J. Zhang, W. Lai and T. Chen, *J. Dairy Sci.*, 2018, **101**, 5770–5779.
28 M. I. Kim, Y. Ye, B. Y. Won, S. Shin, J. Lee and H. G. Park, *Adv. Funct. Mater.*, 2011, **21**, 2868–2875.
29 N. Alizadeh, A. Salimi, R. Hallaj, F. Fathi and F. Soleimani, *Mater. Sci. Eng., C*, 2019, **99**, 1374–1383.
30 H. Fang, Y. Pan, W. Shan, M. Guo, Z. Nie, Y. Huang and S. Yao, *Anal. Methods*, 2014, **6**, 6073–6081.
31 Q. Wang, J. Lei, S. Deng, L. Zhang and H. Ju, *Chem. Commun.*, 2013, **49**, 916–918.
32 H. Wei and E. Wang, *Chem. Soc. Rev.*, 2013, **42**, 6060–6093.
33 H. Sun, Y. Zhou, J. Ren and X. Qu, *Angew. Chem., Int. Ed.*, 2018, **57**, 9224–9237.
34 S. Singh, *Biointerphases*, 2016, **11**, 04B202.
35 E. Kuah, S. Toh, J. Yee, Q. Ma and Z. Gao, *Chem. – Eur. J.*, 2016, **22**, 8404–8430.
36 J. Golchin, K. Golchin, N. Alidadian, S. Ghaderi, S. Eslamkhah, M. Eslamkhah and A. Akbarzadeh, *Artif. Cells, Nanomed., Biotechnol.*, 2017, **45**, 1069–1076.
37 Q. Wang, H. Wei, Z. Zhang, E. Wang and S. Dong, *TrAC, Trends Anal. Chem.*, 2018, **105**, 218–224.
38 J. Wu, S. Li and H. Wei, *Chem. Commun.*, 2018, **54**, 6520–6530.
39 X. Wang, Y. Hu and H. Wei, *Inorg. Chem. Front.*, 2016, **3**, 41–60.
40 S. Lin, J. Wu, J. Yao, W. Cao, F. Muhammad and H. Wei, *Nanozymes for Biomedical Sensing Applications: From In Vitro to Living Systems*, Elsevier Inc., 2018.
41 W. Zheng and X. Jiang, *Analyst*, 2016, **141**, 1196–1208.

42 M. Liang and X. Yan, *Acc. Chem. Res.*, 2019, **52**, 2190–2200.
43 X. Yan, *Nanozymology: Connecting Biology and Nanotechnology*, Springer, Singapore, 2020.
44 S. H. H. Shokouh, A. Pezeshki, S. R. A. Raza, K. Choi, S.-W. Min, P. J. Jeon, H. S. Lee and S. Im, *ACS Nano*, 2014, **8**, 5174–5181.
45 R. Bonomi, A. Cazzolaro, A. Sansone, P. Scrimin and L. J. Prins, *Angew. Chem., Int. Ed.*, 2011, **50**, 2307–2312.
46 L. Pasquato, F. Rancan, P. Scrimin, F. Mancin and C. Frigeri, *Chem. Commun.*, 2000, **2**, 2253–2254.
47 P. Pengo, S. Polizzi, L. Pasquato and P. Scrimin, *J. Am. Chem. Soc.*, 2005, **127**, 1616–1617.
48 S. Singh, *Front. Chem.*, 2019, **7**, 46.
49 A. Rahal, A. Kumar, V. Singh, B. Yadav, R. Tiwari, S. Chakraborty and K. Dhama, *BioMed Res. Int.*, 2014, **2014**, 761264.
50 R. Das, A. Dhiman, A. Kapil, V. Bansal and T. K. Sharma, *Anal. Bioanal. Chem.*, 2019, **411**, 1229–1238.
51 J. Wang, X. Jiao Chen, K. Ming Liao, G. Hou Wang and M. Han, *Nanoscale Res. Lett.*, 2015, **10**, 1–6.
52 S. Tanaka, Y. V. Kaneti, R. Bhattacharjee, M. N. Islam, R. Nakahata, N. Abdullah, S. I. Yusa, N.-T. Nguyen, M. J. A. Shiddiky, Y. Yamauchi and M. S. A. Hossain, *ACS Appl. Mater. Interfaces*, 2018, **10**, 1039–1049.
53 R. Bhattacharjee, S. Tanaka, S. Moriam, M. K. Masud, J. Lin, S. M. Alshehri, T. Ahamad, R. R. Salunkhe, N.-T. Nguyen, Y. Yamauchi, M. S. A. Hossain and M. J. A. Shiddiky, *J. Mater. Chem. B*, 2018, **6**, 4783–4791.
54 M. K. Masud, S. Yadav, M. N. Islam, N.-T. Nguyen, C. Salomon, R. Kline, H. R. Alamri, Z. A. Alothman, Y. Yamauchi, M. S. A. Hossain and M. J. A. Shiddiky, *Anal. Chem.*, 2017, **89**, 11005–11013.
55 K. Boriachek, M. K. Masud, C. Palma, H.-P. Phan, Y. Yamauchi, M. S. A. Hossain, N.-T. Nguyen, C. Salomon and M. J. A. Shiddiky, *Anal. Chem.*, 2019, **91**, 3827–3834.
56 Z. Zhang, H. Zhu, X. Wang and X. Yang, *Microchim. Acta*, 2011, **174**, 183–189.
57 J. Mu, X. Zhao, J. Li, E. C. Yang and X. J. Zhao, *Mater. Sci. Eng., C*, 2017, **74**, 434–442.
58 L. Tian, J. Qi, K. Qian, O. Oderinde, Q. Liu, C. Yao, W. Song and Y. Wang, *J. Electroanal. Chem.*, 2018, **812**, 1–9.
59 K. Shim, W. C. Lee, M. S. Park, M. Shahabuddin, Y. Yamauchi, M. S. A. Hossain, Y.-B. Shim and J. H. Kim, *Sens. Actuators, B*, 2019, **278**, 88–96.
60 M. H. Naveen, N. G. Gurudatt, H. B. Noh and Y.-B. Shim, *Adv. Funct. Mater.*, 2016, **26**, 1590–1601.
61 H. B. Noh, K. S. Lee, P. Chandra, M. S. Won and Y.-B. Shim, *Electrochim. Acta*, 2012, **61**, 36–43.
62 G. H. Jin, E. Ko, M. K. Kim, V. K. Tran, S. E. Son, Y. Geng, W. Hur and G. H. Seong, *Sens. Actuators, B*, 2018, **274**, 201–209.
63 L. Liu, J. Du, W.-E. Liu, Y. Guo, G. Wu, W. Qi and X. Lu, *Anal. Bioanal. Chem.*, 2019, **411**, 2189–2200.
64 A. Umar, S. Kim, R. Kumar, H. Algarni and M. S. Al-Assiri, *Ceram. Int.*, 2016, **42**, 9257–9263.
65 L. Cui, J. Wu, J. Li and H. Ju, *Anal. Chem.*, 2015, **87**, 10635–10641.
66 N. Yu, Z. Wang, C. Wang, J. Han and H. Bu, *Anal. Chim. Acta*, 2017, **962**, 24–31.
67 Y. Li, C. Yu, B. Yang, Z. Liu, P. Xia and Q. Wang, *Biosens. Bioelectron.*, 2018, **102**, 307–315.
68 L. Tian, J. Qi, O. Oderinde, C. Yao, W. Song and Y. Wang, *Biosens. Bioelectron.*, 2018, **110**, 110–117.
69 P. Ling, J. Lei, L. Zhang and H. Ju, *Anal. Chem.*, 2015, **87**, 3957–3963.
70 X. Hun, G. Xie and X. Luo, *Chem. Commun.*, 2015, **51**, 7100–7103.
71 G.-Y. Zhang, S.-Y. Deng, W.-R. Cai, S. Cosnier, X.-J. Zhang and D. Shan, *Anal. Chem.*, 2015, **87**, 9093–9100.
72 L. Shi, Y. Yu, Z. Chen, L. Zhang, S. He, Q. Shi and H. Yang, *RSC Adv.*, 2015, **5**, 11541–11548.
73 S. Yadav, M. K. Masud, M. N. Islam, V. Gopalan, A. K.-Y. Lam, S. Tanaka, N.-T. Nguyen, M. S. A. Hossain, C. Li, Y. Yamauchi and M. J. A. Shiddiky, *Nanoscale*, 2017, **9**, 8805–8814.
74 D. Sun, X. Lin, J. Lu, P. Wei, Z. Luo, X. Lu, Z. Chen and L. Zhang, *Biosens. Bioelectron.*, 2019, **142**, 111578.
75 D. Sun, Z. Luo, J. Lu, S. Zhang, T. Che, Z. Chen and L. Zhang, *Biosens. Bioelectron.*, 2019, **134**, 49–56.
76 D. Ou, D. Sun, X. Lin, Z. Liang, Y. Zhong and Z. Chen, *J. Mater. Chem. B*, 2019, **7**, 3661–3669.
77 L. Jiao, Z. Mu, L. Miao, W. Du, Q. Wei and H. Li, *Microchim. Acta*, 2017, **184**, 423–429.
78 T. Zhang, Y. Song, Y. Xing, Y. Gu, X. Yan, H. Liu, N. Lu, H. Xu, Z. Xu, Z. Zhang and M. Yang, *Nanoscale*, 2019, **11**, 20221–20227.
79 Y. Wang, Y. Wang, X. Pang, B. Du, H. Li, D. Wu and Q. Wei, *Sens. Actuators, B*, 2015, **214**, 124–131.
80 P. Ling, C. Qian, J. Yu and F. Gao, *Biosens. Bioelectron.*, 2020, **149**, 111838.
81 J. Xi, C. Xie, Y. Zhang, L. Wang, J. Xiao, X. Duan, J. Ren, F. Xiao and S. Wang, *ACS Appl. Mater. Interfaces*, 2016, **8**, 22563–22573.
82 L. Tian, J. Qi, K. Qian, O. Oderinde, Y. Cai, C. Yao, W. Song and Y. Wang, *Sens. Actuators, B*, 2018, **260**, 676–684.
83 S. Savas and Z. Altintas, *Materials*, 2019, **12**, 2189.
84 M.-Q. Wang, C. Ye, S.-J. Bao, M.-W. Xu, Y. Zhang, L. Wang, X.-Q. Ma, J. Guo and C.-M. Li, *Biosens. Bioelectron.*, 2017, **87**, 998–1004.
85 X. Cai, Z. Wang, H. Zhang, Y. Li, K. Chen, H. Zhao and M. Lan, *J. Mater. Chem. B*, 2019, **7**, 401–407.
86 X. Chen, D. Liu, G. Cao, Y. Tang and C. Wu, *ACS Appl. Mater. Interfaces*, 2019, **11**, 9374–9384.
87 S. E. Son, E. Ko, V.-K. Tran, W. Hur, H. Choi, H. B. Lee, Y. Park and G. H. Seong, *ChemElectroChem*, 2019, **6**, 4666–4673.
88 J. Zhu, X. Peng, W. Nie, Y. Wang, J. Gao, W. Wen, J. N. Selvaraj, X. Zhang and S. Wang, *Biosens. Bioelectron.*, 2019, **141**, 111450.
89 K. Wang, C. Wu, F. Wang, M. Liao and G. Jiang, *Biosens. Bioelectron.*, 2020, **150**, 111869.

90 J. W. Lee, H. J. Jeon, H.-J. Shin and J. K. Kang, *Chem. Commun.*, 2012, **48**, 422–424.
91 N. Puvvada, P. K. Panigrahi, D. Mandal and A. Pathak, *RSC Adv.*, 2012, **2**, 3270–3273.
92 C. Ge, G. Fang, X. Shen, Y. Chong, W. G. Wamer, X. Gao, Z. Chai, C. Chen and J.-J. Yin, *ACS Nano*, 2016, **10**, 10436–10445.
93 S. Wang, W. Chen, A. L. Liu, L. Hong, H. H. Deng and X. H. Lin, *ChemPhysChem*, 2012, **13**, 1199–1204.
94 N. Abu Tarboush, L. M. R. Jensen, M. Feng, H. Tachikawa, C. M. Wilmot and V. L. Davidson, *Biochemistry*, 2010, **49**, 9783–9791.
95 J. Xu, H. Yang, W. Fu, K. Du, Y. Sui, J. Chen, Y. Zeng, M. Li and G. Zou, *J. Magn. Magn. Mater.*, 2007, **309**, 307–311.
96 N. M. A. Rashid, C. Haw, W. Chiu, N. H. Khanis, A. Rohaizad, P. Khiew and S. A. Rahman, *CrystEngComm*, 2016, **18**, 4720–4732.
97 J. Park, K. An, Y. Hwang, J.-G. Park, H.-J. Noh, J.-Y. Kim, J.-H. Park, N.-M. Hwang and T. Hyeon, *Nat. Mater.*, 2004, **3**, 891–895.
98 S. Sun, H. Zeng, D. B. Robinson, S. Raoux, P. M. Rice, S. X. Wang and G. Li, *J. Am. Chem. Soc.*, 2004, **126**, 273–279.
99 M. E. Franke, T. J. Koplin and U. Simon, *Small*, 2006, **2**, 36–50.
100 S. Brovelli, N. Chiodini, R. Lorenzi, A. Lauria, M. Romagnoli and A. Paleari, *Nat. Commun.*, 2012, **3**, 690.
101 Z. Zhang, C. Dong, C. Yang, D. Hu, J. Long, L. Wang, H. Li, Y. Chen and D. Kong, *Adv. Synth. Catal.*, 2010, **352**, 1600–1604.
102 V. Urbanova, M. Magro, A. Gedanken, D. Baratella, F. Vianello and R. Zboril, *Chem. Mater.*, 2014, **26**, 6653–6673.
103 H. D. Yu, M. D. Regulacio, E. Ye and M. Y. Han, *Chem. Soc. Rev.*, 2013, **42**, 6006–6018.
104 M. Ambrosi, E. Fratini, P. Canton, S. Dankesreiter and P. Baglioni, *J. Mater. Chem.*, 2012, **22**, 23497–23505.
105 A. M. Ealias and M. P. Saravanakumar, *IOP Conf. Ser.: Mater. Sci. Eng.*, 2017, **263**, 032019.
106 S. Sun, H. Zeng, D. B. Robinson, S. Raoux, P. M. Rice, S. X. Wang and G. Li, *J. Am. Chem. Soc.*, 2004, **126**, 273–279.
107 F. Zhao, B. Zhang and L. Feng, *Mater. Lett.*, 2012, **68**, 112–114.
108 H. Cui and W. Ren, *J. Sol-Gel Sci. Technol.*, 2008, **47**, 81–84.
109 H. Qi, B. Yan, W. Lu, C. Li and Y. Yang, *Curr. Nanosci.*, 2011, **7**, 381–388.
110 M. Sangermano, P. Allia, P. Tiberto, G. Barrera, F. Bondioli, N. Florini and M. Messori, *Macromol. Chem. Phys.*, 2013, **214**, 508–516.
111 H. Cui, Y. Liu and W. Ren, *Adv. Powder Technol.*, 2013, **24**, 93–97.
112 X.-L. Li, Q. Peng, J.-X. Yi, X. Wang and Y. Li, *Chem. – Eur. J.*, 2006, **12**, 2383–2391.
113 X. Hu, J. Gong, L. Zhang and J. C. Yu, *Adv. Mater.*, 2008, **20**, 4845–4850.
114 W.-W. Wang, Y.-J. Zhu and M.-L. Ruan, *J. Nanopart. Res.*, 2007, **9**, 419–426.
115 W.-W. Wang, Y.-J. Zhu, G.-F. Cheng and Y.-H. Huang, *Mater. Lett.*, 2006, **60**, 609–612.
116 A. V. Nikam, A. Arulkashmir, K. Krishnamoorthy, A. A. Kulkarni and B. L. V. Prasad, *Cryst. Growth Des.*, 2014, **14**, 4329–4334.
117 I. Bilecka, I. Djerdj and M. Niederberger, *Chem. Commun.*, 2008, 886–888.
118 M. I. Dar, A. K. Chandiran, M. Grätzel, M. K. Nazeeruddin and S. A. Shivashankar, *J. Mater. Chem. A*, 2014, **2**, 1662–1667.
119 T. Hyeon, S. S. Lee, J. Park, Y. Chung and H. B. Na, *J. Am. Chem. Soc.*, 2001, **123**, 12798–12801.
120 S. Guru, D. Mishra, S. S. Amritphale and S. Joshi, *Colloid Polym. Sci.*, 2016, **294**, 207–213.
121 D. A. Giljohann, D. S. Seferos, W. L. Daniel, M. D. Massich, P. C. Patel and C. A. Mirkin, *Angew. Chem., Int. Ed.*, 2010, **49**, 3280–3294.
122 M. A. Hayat, *Colloidal Gold. Principles, Methods and Applications*, Academic Press, San Diego, London, 1989.
123 J. Turkevich, P. C. Stevenson and J. Hillier, *Discuss. Faraday Soc.*, 1951, **11**, 55–75.
124 J. Bonsak, J. Mayandi, A. Thøgersen, E. S. Marstein and U. Mahalingam, *Phys. Status Solidi C*, 2011, **8**, 924–927.
125 J. W. Guo, T. S. Zhao, J. Prabhuram and C. W. Wong, *Electrochim. Acta*, 2005, **50**, 1973–1983.
126 S. Sali, H. R. Mackey and A. A. Abdala, *Nanomaterials*, 2019, **9**, 769.
127 S. Pei and H. M. Cheng, *Carbon*, 2012, **50**, 3210–3228.
128 B. C. Brodie, *R. Soc. London*, 1858, **149**, 423–429.
129 W. S. Hummers and R. E. Offeman, *J. Am. Chem. Soc.*, 1958, **80**, 1339.
130 M. H. Naveen, H. B. Noh, M. S. Al Hossain, J. H. Kim and Y.-B. Shim, *J. Mater. Chem. A*, 2015, **3**, 5426–5433.
131 D. C. Marcano, D. V. Kosynkin, J. M. Berlin, A. Sinitskii, Z. Sun, A. Slesarev, L. B. Alemany, W. Lu and J. M. Tour, *ACS Nano*, 2010, **4**, 4806–4814.
132 P. P. Brisebois and M. Siaj, *J. Mater. Chem. C*, 2020, **8**, 1517–1547.
133 X. Ruan, D. Liu, X. Niu, Y. Wang, C. D. Simpson, N. Cheng, D. Du and Y. Lin, *Anal. Chem.*, 2019, **91**, 13847–13854.
134 D. Tasis, N. Tagmatarchis, A. Bianco and M. Prato, *Chem. Rev.*, 2006, **106**, 1105–1136.
135 V. Schroeder, S. Savagatrup, M. He, S. Lin and T. M. Swager, *Chem. Rev.*, 2019, **119**, 599–663.
136 Y. Huang, J. Ren and X. Qu, *Chem. Rev.*, 2019, **119**, 4357–4412.
137 H. Wang, P. H. Li, D. Q. Yu, Y. Zhang, Z. Z. Wang, C. Q. Liu, H. Qiu, Z. Liu, J. S. Ren and X. G. Qu, *Nano Lett.*, 2018, **18**, 3344–3351.
138 H. Wang, H. Jiang, S. Wang, W. B. Shi, J. C. He, H. Liu and Y. M. Huang, *RSC Adv.*, 2014, **4**, 45809–45815.

139 A. Hayat, W. Haider, Y. Raza and J. L. Marty, *Talanta*, 2015, **143**, 157–161.

140 H. Wang, S. Li, Y. M. Si, Z. Z. Sun, S. Y. Li and Y. H. Lin, *J. Mater. Chem. B*, 2014, **2**, 4442–4448.

141 J. Qian, X. W. Yang, Z. T. Yang, G. B. Zhu, H. P. Mao and K. Wang, *J. Mater. Chem. B*, 2015, **3**, 1624–1632.

142 Y. F. Zhang, C. L. Xu and B. X. Li, *RSC Adv.*, 2013, **3**, 6044–6050.

143 Y. Lv, M. Ma, Y. Huang and Y. Xia, *Chem. – Eur. J.*, 2019, **25**, 954–960.

144 H. Li, Z. Kang, Y. Liu and S. T. Lee, *J. Mater. Chem.*, 2012, **22**, 24230–24253.

145 X. Wang, Y. Feng, P. Dong and J. Huang, *Front. Chem.*, 2019, **7**, 671.

146 K. Nekoueian, M. Amiri, M. Sillanpää, F. Marken, R. Boukherroub and S. Szunerits, *Chem. Soc. Rev.*, 2019, **48**, 4281–4316.

147 S. Y. Lim, W. Shen and Z. Gao, *Chem. Soc. Rev.*, 2015, **44**, 362–381.

148 M. Shamsipur, A. Safavi and Z. Mohammadpour, *Sens. Actuators, B*, 2014, **199**, 463–469.

149 W. Shi, Q. Wang, Y. Long, Z. Cheng, S. Chen, H. Zheng and Y. Huang, *Chem. Commun.*, 2011, **47**, 6695–6697.

150 Z. Mohammadpour, A. Safavi and M. Shamsipur, *Chem. Eng. J.*, 2014, **255**, 1–7.

151 C. Li, Y. Yang, D. Wu, T. Li, Y. Yin and G. Li, *Chem. Sci.*, 2016, **7**, 3011–3016.

152 Y. Hu, X. J. Gao, Y. Zhu, F. Muhammad, S. Tan, W. Cao, S. Lin, Z. Jin, X. Gao and H. Wei, *Chem. Mater.*, 2018, **30**, 6431–6439.

153 C. N. Loynachan, M. R. Thomas, E. R. Gray, D. A. Richards, J. Kim, B. S. Miller, J. C. Brookes, S. Agarwal, V. Chudasama, R. A. McKendry and M. M. Stevens, *ACS Nano*, 2018, **12**, 279–288.

154 C. J. Yu, C. Y. Lin, C. H. Liu, T. L. Cheng and W. L. Tseng, *Biosens. Bioelectron.*, 2010, **26**, 913–917.

155 M. Il Kim, J. Shim, T. Li, J. Lee and H. G. Park, *Chem. – Eur. J.*, 2011, **17**, 10700–10707.

156 Y. L. Dong, H. G. Zhang, Z. U. Rahman, L. Su, X. J. Chen, J. Hu and X. G. Chen, *Nanoscale*, 2012, **4**, 3969–3976.

157 F. Huang, J. Wang, W. Chen, Y. Wan, X. Wang, N. Cai, J. Liu and F. Yu, *J. Taiwan Inst. Chem. Eng.*, 2018, **83**, 40–49.

158 M. K. Masud, J. Kim, M. M. Billah, K. Wood, M. J. A. Shiddiky, N.-T. Nguyen, R. K. Parsapur, Y. V. Kaneti, A. A. Alshehri, Y. G. Alghamidi, K. A. Alzahrani, M. Adharvanachari, P. Selvam, M. S. A. Hossain and Y. Yamauchi, *J. Mater. Chem. B*, 2019, **7**, 5412–5422.

159 X. Wang, W. Cao, L. Qin, T. Lin, W. Chen, S. Lin, J. Yao, X. Zhao, M. Zhou, C. Hang and H. Wei, *Theranostics*, 2017, **7**, 2277–2286.

160 X. Wang, X. J. Gao, L. Qin, C. Wang, L. Song, Y. N. Zhou, G. Zhu, W. Cao, S. Lin, L. Zhou, K. Wang, H. Zhang, Z. Jin, P. Wang, X. Gao and H. Wei, *Nat. Commun.*, 2019, **10**, 1–8.

161 T. Hossain, G. Mahmudunnabi, M. K. Masud, M. N. Islam, L. Ooi, K. Konstantinov, M. S. Al Hossain, B. Martinac, G. Alici, N.-T. Nguyen and M. J. A. Shiddiky, *Biosens. Bioelectron.*, 2017, **94**, 63–73.

162 J. Shah, R. Purohit, R. Singh, A. S. Karakoti and S. Singh, *J. Colloid Interface Sci.*, 2015, **456**, 100–107.

163 N. De Acha, C. Elosúa, J. M. Corres and F. J. Arregui, *Sensors*, 2019, **19**, 599.

164 R. Zhang, S. He, C. Zhang and W. Chen, *J. Mater. Chem. B*, 2015, **3**, 4146–4154.

165 M. H. Lee, J. S. Kim and J. L. Sessler, *Chem. Soc. Rev.*, 2015, **44**, 4185–4191.

166 W. Deng, Y. Peng, H. Yang, Y. Tan, M. Ma, Q. Xie and S. Chen, *ACS Appl. Mater. Interfaces*, 2019, **11**, 29072–29077.

167 M. H. Naveen, N. G. Gurudatt and Y.-B. Shim, *Appl. Mater. Today*, 2017, **9**, 419–433.

168 E. O. Blair and D. K. Corrigan, *Biosens. Bioelectron.*, 2019, **134**, 57–67.

169 N. Soda, B. H. A. Rehm, P. Sonar, N.-T. Nguyen and M. J. A. Shiddiky, *J. Mater. Chem. B*, 2019, **7**, 6670–6704.

170 M. K. Masud, J. Na, M. Younus, M. S. A. Hossain, Y. Bando, M. J. A. Shiddiky and Y. Yamauchi, *Chem. Soc. Rev.*, 2019, **48**, 5717–5751.

171 K. M. Koo, L. G. Carrascosa, M. J. A. Shiddiky and M. , *Anal. Chem.*, 2016, **88**, 2000–2005.

172 M. N. Islam, M. K. Masud, M. H. Haque, M. S. A. Hossain, Y. Yamauchi, N.-T. Nguyen and M. J. A. Shiddiky, *Small Methods*, 2017, **1**, 1700131.

173 J. Wang, J. Chen and S. Sen, *J. Cell. Physiol.*, 2016, **231**, 25–30.

174 M. N. Islam, L. Gorgannezhad, M. K. Masud, S. Tanaka, M. S. A. Hossain, Y. Yamauchi, N.-T. Nguyen and M. J. A. Shiddiky, *ChemElectroChem*, 2018, **5**, 2488–2495.

175 K. Boriachek, M. Umer, M. N. Islam, V. Gopalan, A. K. Lam, N.-T. Nguyen and M. J. A. Shiddiky, *Analyst*, 2018, **143**, 1662–1669.

176 M. Kamal Masud, M. N. Islam, M. H. Haque, S. Tanaka, V. Gopalan, G. Alici, N.-T. Nguyen, A. K. Lam, M. S. A. Hossain, Y. Yamauchi and M. J. A. Shiddiky, *Chem. Commun.*, 2017, **53**, 8231–8234.

177 M. N. Islam, M. K. Masud, N.-T. Nguyen, V. Gopalan, H. R. Alamri, Z. A. Alothman, M. S. A. Hossain, Y. Yamauchi, A. K. Y. Lam and M. J. A. Shiddiky, *Biosens. Bioelectron.*, 2018, **101**, 275–281.

178 M. N. Islam, M. K. Masud, M. H. Haque, M. S. A. Hossain, Y. Yamauchi, N.-T. Nguyen and M. J. A. Shiddiky, *Small Methods*, 2017, **1**, 1700131.

179 M. Umer, R. Vaidyanathan, N. T. Nguyen and M. J. A. Shiddiky, *Biotechnol. Adv.*, 2018, **36**, 1367–1389.

180 F. S. Felix and L. Angnes, *Biosens. Bioelectron.*, 2018, **102**, 470–478.

181 Y. Li, Y. Zhang, F. Li, J. Feng, M. Li, L. Chen and Y. Dong, *Biosens. Bioelectron.*, 2017, **92**, 33–39.

182 F. Li, Y. Li, J. Feng, Z. Gao, H. Lv, X. Ren and Q. Wei, *Biosens. Bioelectron.*, 2018, **100**, 512–518.

183 L. Zhang, X. Xie, Y. Yuan, Y. Chai and R. Yuan, *Electroanalysis*, 2019, **31**, 1019–1025.

184 M. Jarczewska, Ł. Górski and E. Malinowska, *Anal. Methods*, 2016, **8**, 3861–3877.

185 Y. Zhu, P. Chandra, K. M. Song, C. Ban and Y. B. Shim, *Biosens. Bioelectron.*, 2012, **36**, 29–34.

186 X. Wang, L. Cohen, J. Wang and D. R. Walt, *J. Am. Chem. Soc.*, 2018, **140**, 18132–18139.

187 W. Wang, L. Liu, L. Xu, H. Kuang, J. Zhu and C. Xu, *Part. Part. Syst. Charact.*, 2016, **33**, 388–395.

188 C. Wang, C. Liu, J. Luo, Y. Tian and N. Zhou, *Anal. Chim. Acta*, 2016, **936**, 75–82.

189 D. S. Wishart, *PLoS Comput. Biol.*, 2012, **8**, e1002805.

190 K. J. Cash and H. A. Clark, *Trends Mol. Med.*, 2010, **16**, 584–593.

191 K. Rathee, V. Dhull, R. Dhull and S. Singh, *Biochem. Biophys. Rep.*, 2016, **5**, 35–54.

192 J. Bakker, P. Gris, M. Coffernils, R. J. Kahn and J. L. Vincent, *Am. J. Surg.*, 1996, **171**, 221–226.

193 N. P. Sardesai, M. Ganesana, A. Karimi, J. C. Leiter and S. Andreescu, *Anal. Chem.*, 2015, **87**, 2996–3003.

194 S. Tanaka, Y. V. Kaneti, R. Bhattacharjee, M. N. Islam, R. Nakahata, N. Abdullah, S. I. Yusa, N.-T. Nguyen, M. J. A. Shiddiky, Y. Yamauchi and M. S. A. Hossain, *ACS Appl. Mater. Interfaces*, 2018, **10**, 1039–1049.

195 E. V. Karpova, E. V. Shcherbacheva, A. A. Galushin, D. V. Vokhmyanina, E. E. Karyakina and A. A. Karyakin, *Anal. Chem.*, 2019, **91**, 3778–3783.

196 J. Zhu, X. Peng, W. Nie, Y. Wang, J. Gao, W. Wen, J. N. Selvaraj, X. Zhang and S. Wang, *Biosens. Bioelectron.*, 2019, **141**, 111450.

197 M. Wu, S. Meng, Q. Wang, W. Si, W. Huang and X. Dong, *ACS Appl. Mater. Interfaces*, 2015, **7**, 21089–21094.

198 D. V. Vokhmyanina, K. D. Andreeva, M. A. Komkova, E. E. Karyakina and A. A. Karyakin, *Talanta*, 2020, **208**, 120393.

199 E. V. Karpova, A. I. Laptev, E. A. Andreev, E. E. Karyakina and A. A. Karyakin, *ChemElectroChem*, 2020, **7**, 191–194.

200 K. Wang, C. Wu, F. Wang, M. Liao and G. Jiang, *Biosens. Bioelectron.*, 2020, **150**, 111869.

201 S. H. Wen, X. L. Zhong, Y. Di Wu, R. P. Liang, L. Zhang and J. D. Qiu, *Anal. Chem.*, 2019, **91**, 6487–6497.

202 F. Xiao, L. Wang and H. Duan, *Biotechnol. Adv.*, 2016, **34**, 234–249.

203 Z. Da Gao, Y. Qu, T. Li, N. K. Shrestha and Y. Y. Song, *Sci. Rep.*, 2014, **4**, 6891.

204 M. A. Komkova, E. E. Karyakina and A. A. Karyakin, *J. Am. Chem. Soc.*, 2018, **140**, 11302–11307.

205 G. M. Whitesides, *Nature*, 2006, **442**, 368–373.

206 H. Moghadas, M. S. Saidi, N. Kashaninejad and N.-T. Nguyen, *Drug Delivery Transl. Res.*, 2018, **8**, 830–842.

207 N. Kashaninejad, M. J. A. Shiddiky and N.-T. Nguyen, *Adv. Biosyst.*, 2018, **2**, 1700197.

208 R. Vadivelu, N. Kashaninejad, K. R. Sreejith, R. Bhattacharjee, I. Cock and N.-T. Nguyen, *ACS Appl. Mater. Interfaces*, 2018, **10**, 43439–43449.

209 N. Kashaninejad, M. Yaghoobi, M. Pourhassan-Moghaddam, S. R. Bazaz, D. Jin and M. E. Warkiani, *Nanotechnol. Microfluid*, 2020, pp. 211–238.

210 G.-P. Nikoleli, C. G. Siontorou, D. P. Nikolelis, S. Bratakou, S. Karapetis and N. Tzamtzis, in *Nanotechnology and Biosensors*, ed. D. P. Nikolelis and G.-P. Nikoleli, Elsevier, 2018, pp. 375–394.

211 Y. Song, Y. Zhang, P. E. Bernard, J. M. Reuben, N. T. Ueno, R. B. Arlinghaus, Y. Zu and L. Qin, *Nat. Commun.*, 2012, **3**, 1283.

212 Y. Song, X. Xia, X. Wu, P. Wang and L. Qin, *Angew. Chem., Int. Ed.*, 2014, **53**, 12451–12455.

213 Z. Zhu, Z. Guan, S. Jia, Z. Lei, S. Lin, H. Zhang, Y. Ma, Z.-Q. Tian and C. J. Yang, *Angew. Chem., Int. Ed.*, 2014, **53**, 12503–12507.

214 I. Ortiz-Gómez, A. Salinas-Castillo, A. G. García, J. A. Álvarez-Bermejo, I. de Orbe-Payá, A. Rodríguez-Diéguez and L. F. Capitán-Vallvey, *Microchim. Acta*, 2017, **185**, 47.

215 P. Zhang, D. Sun, A. Cho, S. Weon, S. Lee, J. Lee, J. W. Han, D.-P. Kim and W. Choi, *Nat. Commun.*, 2019, **10**, 940.

216 H. Cheng, L. Zhang, J. He, W. Guo, Z. Zhou, X. Zhang, S. Nie and H. Wei, *Anal. Chem.*, 2016, **88**, 5489–5497.

217 R. Shen, P. Liu, Y. Zhang, Z. Yu, X. Chen, L. Zhou, B. Nie, A. Żaczek, J. Chen and J. Liu, *Anal. Chem.*, 2018, **90**, 4478–4484.

218 K. M. Koo, S. Dey and M. Trau, *ACS Sens.*, 2018, **3**, 2597–2603.

219 E. Ko, V.-K. Tran, S. E. Son, W. Hur, H. Choi and G. H. Seong, *Sens. Actuators, B*, 2019, **294**, 166–176.

220 Z. Zhang, Y. Li, X. Zhang and J. Liu, *Nanoscale*, 2019, **11**, 4854–4863.

221 X. Lian, Y. Fang, E. Joseph, Q. Wang, J. Li, S. Banerjee, C. Lollar, X. Wang and H.-C. Zhou, *Chem. Soc. Rev.*, 2017, **46**, 3386–3401.

222 N. Liu, Z. Xu, A. Morrin and X. Luo, *Anal. Methods*, 2019, **11**, 702–711.

223 N.-T. Nguyen, M. Hejazian, C. H. Ooi and N. Kashaninejad, *Micromachines*, 2017, **8**, 186.

224 P. Rostami, N. Kashaninejad, K. Moshksayan, M. S. Saidi, B. Firoozabadi and N.-T. Nguyen, *J. Sci.: Adv. Mater. Devices*, 2019, **4**, 1–18.

225 S. Yadav, N. Kashaninejad, M. K. Masud, Y. Yamauchi, N.-T. Nguyen and M. J. A. Shiddiky, *Biosens. Bioelectron.*, 2019, **139**, 111315.